Journal of Materials Chemistry B

ROYAL SOCIETY OF CHEMISTRY

REVIEW

View Article Online
View Journal | View Issue

Cite this: J. Mater. Chem. B, 2023, 11, 5301

Chemical tunability of advanced materials used in the fabrication of micro/nanobots

Saloni Andhari,[ab] Ganesh Khutale,[ab] Rituja Gupta,[c] Yuvraj Patil[c] and Jayant Khandare *[abcdef]

Received 16th December 2022,
Accepted 11th April 2023

DOI: 10.1039/d2tb02743g

rsc.li/materials-b

Micro and nanobots (MNBs) are unprecedented in their ability to be chemically tuned for autonomous tasks with enhanced targeting and functionality while maintaining their mobility. A myriad of chemical modifications involving a large variety of advanced materials have been demonstrated to be effective in the design of MNBs. Furthermore, they can be controlled for their autonomous motion, and their ability to carry chemical or biological payloads. In addition, MNBs can be modified to achieve targetability with specificity for biological implications. MNBs by virtue of their chemical compositions may be limited by their biocompatibility, tissue accumulation, poor biodegradability and toxicity. This review presents a note on artificial intelligence materials (AIMs), their importance, and the dimensional scales at which intrinsic autonomy can be achieved for diverse utility. We briefly discuss the evolution of such systems with a focus on their advancements in nanomedicine. We highlight MNBs covering their contemporary traits and the emergence of a few start-ups in specific areas. Furthermore, we showcase various examples, demonstrating that chemical tunability is an attractive primary approach for designing MNBs with immense capabilities both in biology and chemistry. Finally, we cover biosafety and ethical considerations in designing MNBs in the era of artificial intelligence for varied applications.

10th Anniversary Statement

As the esteemed journal, *'Journal of Materials Chemistry B'* completes its first decade, we look back upon our mutual timelines and feel glad for the opportunity to be associated with one of the leading scientific periodicals reporting on the latest advances in chemistry within the realm of health sciences. In fact, our work, published with the *Journal of Materials Chemistry B* in the last few years, maps our co-evolution with a transition from exploring anti-cancer targeting nanoparticles to exploring the very nature of the cancer cell and then on to the development of advanced systems to diagnose circulating tumor cells in at-risk individuals till the current milestone of reviewing micro/nanobots and summarizing our decade of work in the field. In the true spirit of scientific advancement, *Journal of Materials Chemistry B* promotes and indeed attracts the leading wave of applied chemical research. With a diverse bouquet of topics covering diagnostics, anti-cancer therapeutics, bone and tissue regeneration, biosensors to fundamental materials research, *Journal of Materials Chemistry B* represents the cutting edge of technological research and we congratulate the *Journal of Materials Chemistry B* on 10 wonderful years of publishing and enriching translational science.

1. Introduction

The transformation of advanced nanomaterials into novel micro and nanobots (MNBs) has led to an exponential increase in their capabilities, both in chemical and biological sciences.[1] Thus, designing autonomous intelligent devices/machines that can perform tasks under minimal external supervision has captured researchers' interests and attention. MNBs can thus be considered as "artificial intelligence materials (AIMs)", governed by physico-chemical traits for superior applications. Such materials can enable possibilities that have never been articulated, in particular where the human intervention is expected to be minimal. Autonomous robots at the macro-scale have alleviated human efforts in diverse fields including, space exploration, industrial manufacturing units and transportation.[2–4] However, in the biomedical field, robots at the micro/nano-scale and even molecular scale are sought after owing to the manoeuvrability of the robots and their ease of

[a] OneCell Diagnostics, Pune 411057, India
[b] OneCell Diagnostics, Cupertino, California 95014, USA
[c] School of Pharmacy, Dr. Vishwanath Karad MIT World Peace University, Kothrud, Pune 411038, India. E-mail: jayant.khandare@mippune.edu.in
[d] Actorius Innovations and Research, Pune, 411057, India
[e] Actorius Innovations and Research, Simi Valley, CA 93063, USA
[f] School of Consciousness, Dr. Vishwanath Karad MIT World Peace University, Kothrud, Pune 411038, India

accessibility (Fig. 1). Thus, the scale of autonomous machines depending on their applications is diverse, ranging from several feet long to as small as a few atoms in dimension (Fig. 2a–f).

Through a variety of approaches, MNBs exhibiting diverse architectures including nanorods/wires, microtubes, two-dimensional (2D) plates and Janus nanoparticles (NPs) have been designed by rolling-up, template-based or self-assembly techniques.[5–9]

Several microorganisms, for instance, motile bacteria, have locomotory capacity, which is an evolutionary necessity to reach nutrients/safety, and have been developed through exposure to a variety of aqueous environments, complex biological media and stimuli.[10] On the other hand, in most multicellular animals, circulatory systems prevail, which carry out nutrient supply and waste handling functions across the entire body, and also bear micro-particulates with diverse functions. Blood micro-particulates have evolved by size, shape, biochemical functionality and intended polyfunctional physiological role such as differential surface glycosyl chemistry in the multitude of blood cells.[11,12] The varying surface chemistry further impacts their stability and circulatory lifetime, which in turn correlates with their physiological function. However, unlike unicellular organisms, blood micro-particulates have limited control over their motion and are largely influenced by circulatory fluid dynamics. Notable exceptions are polymorphonuclear cells such as neutrophils which can self-propel under microbial-chemotactic influence.[13]

Saloni Andhari

Saloni Andhari received her PhD degree in Pharmaceutics from MAEER's Maharashtra Institute of Pharmacy, Savitribai Phule Pune University, India. Her doctoral work focused on the development of autonomously propelled micro-rockets as advanced drug delivery systems that display complex chemo-mechanics with applications in targeted drug delivery. Currently, she is a Postdoctoral Research Fellow at OneCell Diagnostics, India. Her research interests include the detection and isolation of circulating tumor cells, 3D cell culture and the design of nanorobots and advanced nanomaterials for cancer therapeutics.

Ganesh Khutale

Ganesh Khutale received his PhD degree in Nano Drug Delivery Systems from Technological University Dublin, Ireland. During his PhD studies, he worked on the development of gold nanoparticle-based drug delivery systems for therapeutic purposes. Prior to his PhD studies, he was a Research Associate at Actorius Innovations and Research, India, involved in the development of iron oxide-based nanosystems for the detection of circulating tumor cells called OncoDiscover® technology. He is a Senior Research Scientist at OneCell Diagnostics India. His current research interests are focused on developing cutting edge biomaterials for the isolation of single circulating tumor cells, cancer diagnostics and therapeutics.

Rituja Gupta

Rituja Gupta earned her Master of Pharmacy degree in Pharmaceutics from Savitribai Phule Pune University, India. Currently, she is a PhD scholar at School of Pharmacy, Dr Vishwanath Karad MIT World Peace University, India. Her PhD project is focused on the design and development of polymeric 3D inverse substrates for therapeutics. Prior to her PhD, she was a Research Associate at Actorius Innovations and Research, India, involved in the development of a novel hydrodynamic polymer system for time-specific and site-specific drug delivery. Her research interests include materials chemistry, targeted drug delivery, microfluidics, glass chemistry and pharmacokinetic/pharmacodynamic studies.

Yuvraj Patil

Yuvraj Patil is an Associate Professor at the School of Pharmacy, Dr Vishwanath Karad MIT World Peace University, India. He received his PhD in Biological Sciences from Louisiana State University, Baton Rouge, USA. He was a postdoctoral fellow at Pennington Biomedical Research Center, USA. Yuvraj has served earlier as the Technical Head at Skeiron Group's mRNA based onco-vaccine unit. Previously, he worked with the MIMER Medical School, India as a Research Faculty. His research interests are in metabolism, endocrinology, cancer biology, nanotherapeutics and diagnostics. Currently, Yuvraj is exploring multifunctional nanomaterials with applications in diagnostics, anticancer therapy and 3D cell culture.

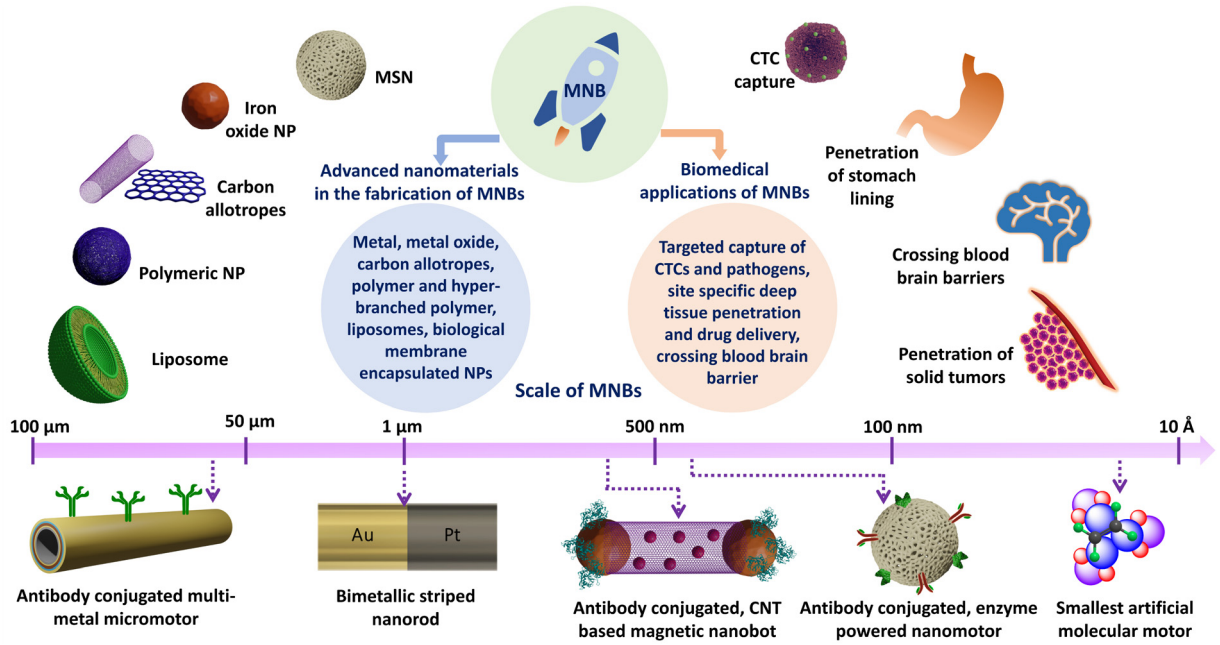

Fig. 1 Schematics of the types of advanced materials used in the fabrication of nanobots, their biomedical applications and their size range. MNBs: micro-nanobots; CTCs: circulating tumor cells; CNT: carbon nanotube; NPs: nanoparticles; MSN: mesoporous silica nanoparticle.

Similarly, bio-hybrid MNBs utilizing bio-motor bearing organisms such as *Escherichia coli* bound to cargo-carrying erythrocytes successfully exploit these evolutionary designs for effective drug delivery.[14] Similarly, sperm-like, flagellar motility has been shown to be utilized by micromotors for the successful delivery of anticancer compounds to tumors.[15] A recent example utilizes chimeric antigen receptor T (CAR T) cells to cloak immunomagnetic beads using click chemistry for antitumor immunoactivation.[16] Despite the advantages of using a biologically inspired or a bio-hybrid MNB such as biological masking, anti-fouling, immune-evasive, and longer circulatory lifetimes, a steady focus on innovating chemically diverse MNBs is sustained by virtue of reproducibility in the fabrication steps and the ability to be chemically tuned for surface modifications.[17]

Prior to the use of MNBs, nanotherapeutic materials demonstrated limited control over their motion and were influenced by the dynamics of blood circulation, affecting their overall pharmacokinetics (PK) and pharmacodynamics (PD). The past few decades have seen a broad exploration of myriad materials in the pursuit of superior MNBs to overcome the drawbacks of "passive" or "static" nanotherapeutics. The primary utility of MNBs is in their locomotory and payload-carrying capacity.

MNBs comprising motor segments are responsible for their active motion and a cargo-carrying segment is vital to perform the intended task. The motor segments consist of metals and metal oxides as catalysts. The metals include, platinum, copper, gold, nickel, silver, magnesium and zinc.[18–27] The metal oxides commonly used in MNBs include calcium carbonate, manganese oxide, iron oxides and zinc oxide.[28–34] Biomolecules such as enzymes have also been utilized as motors, for example catalase, glucose oxidase, urease, acetylcholinesterase, aldolase, laccase and lipase.[35–38]

The cargo carrying segments comprise advanced materials including carbon nanotubes, mesoporous silica, graphene, polymeric nanoparticles (NPs), liposomes and even biohybrid systems wherein a biological membrane/moiety encapsulates advanced nanomaterials for protection against immunological responses.[30,31,39–44] MNBs are particularly being investigated for their ability to autonomously propel, target and selectively discharge pharmacologically active payloads in disease models.

Macro-particulates driven by fluid dynamics involve inertial forces, and thus relatively larger objects move through fluids at

Jayant Khandare

Jayant Khandare is a Professor at the School of Pharmacy and Director at the School of Consciousness, Dr Vishwanath Karad MIT World Peace University, India. He is the Chief Scientific Officer and co-founder of Actorius Innovations and Research, India and USA and OneCell Diagnostics, India and USA. He has a PhD from National Chemical Laboratory, India. He is a recipient of an Alexander von Humboldt Experienced Fellowship at Freie Universität, Germany. His research interests include precision oncology, single-cell omics and designing anticancer drug delivery platforms. He has clinically translated the OncoDiscover® Circulating Tumor Cells Technology from lab to clinics.

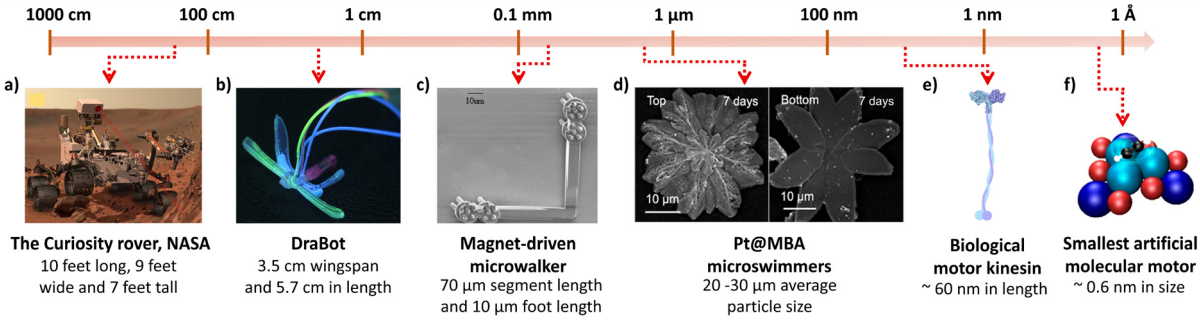

Fig. 2 The dimension scale represents the designs of autonomous robots used in different scientific fields such as space and biomedical engineering. (a) Curiosity rover. Reprinted from ref. 45, Copyright 2018, with permission from Elsevier. (b) DraBot. Reprinted from ref. 46. (c) Magnet-driven microwalker. Reprinted from ref. 47. (d) Platinum deposited melamine barbiturate (Pt@MBA) micro-swimmers. Reprinted from ref. 48. (e) Biological motor kinesin. Reprinted from ref. 49. (f) Smallest artificial molecular motor. Reproduced from ref. 50, with permission from Proceedings of National Academy of Sciences.

a high Reynolds number (Re).[51] Re can be defined using the mathematical expression,

$$\mathrm{Re} = \frac{\rho U L}{\mu}.$$

where U is the velocity of the object relative to the flow, L is the dimension of the object, and ρ and μ are the density and dynamic viscosity of the fluid, respectively.[52] At the micron-level, inertial forces are minuscule while viscous forces dominate. Micron and sub-micron sized objects are subject to fluidic motion at ultra-low Re which was explained by Purcell in his famous talk "Life at low Reynolds number" (Fig. 3). Additionally, the Stokes law is utilized to determine the drag force (F_{drag}) acting on microspheres moving in unbound fluids and is represented by the equation,

$$F_{\mathrm{drag}} = 6\pi\mu r v$$

where μ represents the fluid viscosity, r is the radius of the microsphere and v is the velocity of the microsphere.[53]

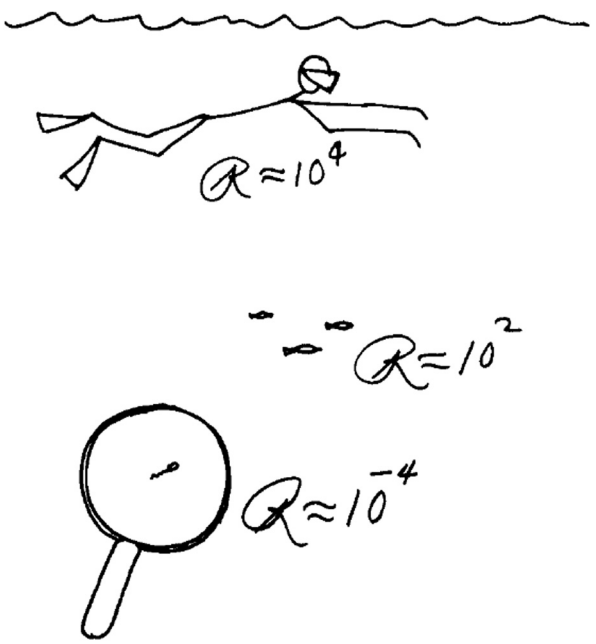

Fig. 3 Scheme from the original transparencies of Purcell's famous talk in 1977 titled "Life at low Reynolds number" comparing Re of objects (a man, fish and sperm swimming in water) with varying dimensions (here, R was used to represent Re). Reproduced from ref. 54, with the permission of the American Association of Physics Teachers.

The primary challenges perceived by contemporary researchers in the area are the appropriate mode of propulsion and guidance/manoeuvrability in complex media/fluids. Furthermore, despite polyfunctional chemistry, the downscaling of small particles or bots is accompanied by a decrease in functionality.[1] These fundamental issues hinge on the intended application and the practicality of the route of administration. Alternative strategies have been explored to compensate for the size reduction, such as microbot swarming; however, these entail additional physical complexities.[55] Approaches employing modifications of surface chemistry are emerging as readily tunable factors which can be employed to achieve the desired functionality given the dimensional restrictions.

Furthermore, studies on "static" nanoparticles (NPs) have revealed that the *in vivo* administration of NPs is subject to differential tissue behaviour at target sites, leading to poor extravasation and tissue penetration, especially in diseased states. While smaller NPs are able to overcome penetration issues and demonstrate higher diffusion coefficients, they are also subject to renal clearance, reducing their effectiveness.[56]

More specifically, surface properties, such as size, shape, surface charge, hydrophobicity and surface chemistry,[57–59] are known to affect the NP performance. Therefore, studying the propulsion traits and surface charge of MNBs in biologically relevant media is essential. The evaluation of the physicochemical traits of MNBs provides guidelines for the development of futuristic MNBs for *in vivo* utility. From previous reports, it is evident that the surface properties and the propulsion kinetics of MNBs are primarily governed by their chemical compositions as shown in Table 1. A thorough study of Table 1 also illustrates that not all reports in the literature

Table 1 List detailing MNBs triggered by different stimuli inducing autonomous propulsion in biologically relevant media and their surface charges

No.	Carrier segment/ advanced materials	Motor segment/ substrate	Stimuli	Dimension of MNBs	Surface charge (medium of measurement)	Maximum speed/MSD/D_e (medium of measurement)	Applications	Ref.
1.	MWCNTs	Fe_3O_4 NPs (D = 16 nm)	H_2O_2 and magnetic field	L = 1 μm; ID = 11 nm	−22.2 mV (PBS)	Speed = 8.0 mm s^{-1} (serum), 2.3 mm s^{-1} (DMEM), 0.9 mm s^{-1} (PBS)	Targeted cellular delivery of drugs and tissue penetration	31
2.	PSBMA	L-Cysteine	H_2S (generated by reaction of L-cysteine with CBS enzyme)	220 nm	−18.9 mV (PBS)	Speed = 5 to 6 μm s^{-1} (cell suspension)	Inhibition of tumor growth	65
3.	Liposomes	Urease	Urea	LB-I: mean R = 100.7 ± 0.5 nm, LB-O: mean R = 105.7 ± 0.8 nm	LB-I: 18.6 ± 1.0 mV, LB-O: −11.8 ± 0.4 mV (PBS)	D_e of LB-I ≈ 6.8 $\mu m^2 s^{-1}$ (PBS in the presence of 0.75% w/v deoxycholate)	Active drug delivery in different *in vivo* locations, such as in the GI tract	43
4.	MSNs	Pt, Au NPs	H_2O_2 and irradiation at 670 nm	Mean D = 495 ± 20 nm	−16.3 mV (PBS)	D_e = 2.97 $\mu m^2 s^{-1}$ (3% H_2O_2) D_e with and without irradiation = 1.26 $\mu m^2 s^{-1}$ and 0.56 $\mu m^2 s^{-1}$ (DI water)	Smart nanomachines responsive to biological stimuli with multiple and tunable propulsion modes	66
5.	DNA barrel	DNA	Freely diffusible ssDNA	L = 40 nm, D = 40 nm	NA	NA	Management of thrombin function in different medical scenarios	67
6.	MSNs	Lipase	Triacetin	D = 413.28 ± 2.77 nm	MSN (−19.36 ± 2.15 mV), MSN-APTES (16.15 ± 1.43 mV), MSN-APTES/GA (−7.2 ± 2.15 mV), MSN-OTES (−13.7 ± 2.27 mV) (PBS), charge on final nanorobots NA	D_e ≈ 1.2 $\mu m^2 s^{-1}$ (PBS) for MSNs with OTES linker	Enzyme powered motors for fine modulation in biomedical and environmental fields	68
7.	β-CD, CdS quantum dots	Ni and Pt tubular microrockets	H_2O_2 and magnetic field	L = 10–20 μm, D = 2–3 μm	0.64 mV (PBS)	Speed = 165 μm s^{-1} (aqueous solution of H_2O_2)	Supramolecular cargo platforms in the field of analytical chemistry, sensors, electronic devices and biomedicine	69
8.	HPAM	L-Arginine	H_2O_2 and NO (ROS)	HLA_n nanomotors D = 120 (HLA_5), 170 (HLA_{10}) and 385 (HLA_{15}) nm	NA	Speed = 3 μm s^{-1} (HLA_{10}), 8 μm s^{-1} (HLA_{15}), 13 μm s^{-1} (HLA_{20}) (aqueous)	Treatment of various diseases in different tissues including blood vessels and tumors	70
9.	Heparin/folic acid	L-Arginine	NO and ROS	HF = 30 nm, HFLA = 35 nm, HFLA-DOX = 50 nm	HF = −51.3 mV, HFLA = −33.9 mV (NA)	MSD ≈ 40 μm^2	Bionic zero waste nanomotor for tumor recognition, facilitated penetration, reversal of MDR, and elimination of tumor	71

Table 1 (*continued*)

No.	Carrier segment/ advanced materials	Motor segment/ substrate	Stimuli	Dimension of MNBs	Surface charge (medium of measurement)	Maximum speed/MSD/D_e (medium of measurement)	Applications	Ref.
10.	Liposomes	MTB	Magnetic field	Bacterium = 0.45–1.8 μm, liposome = 200 nm	Liposome = 39.8 ± 0.9 mV	NA	Delivery of a wide variety of therapeutic cargoes; to overcome persistent transport barriers and improve cancer treatment	72
11.	Janus hollow MSN	Urease and Fe	Urea and magnetic field	D (HP) = 2.32 ± 0.03 μm, ID (mesopores) = 2.17 nm, T (HP) = 77 ± 4 nm	−24 ± 4 mV	Speed = 5 body lengths/s (~10 μm s^{-1}) (aqueous solution of urea)	Transportation of cargoes of different sizes to target locations; targeted drug delivery in biomedical field	73
12.	Liposome	Molecular motor	UV-irradiation	~170 nm	−10 mV	Speed of molecular rotations not mentioned	Facilitate on-demand release; reduce drug toxicity and improve therapeutic efficacy	74

MSD: mean squared displacement; D_e: diffusion co-efficient; MWCNTs: multi-walled carbon nanotubes; D: diameter; Fe_3O_4: ferrous ferric oxide; NPs: nanoparticles; H_2O_2: hydrogen peroxide; L = length; ID: internal diameter; PBS: phosphate buffered saline; DMEM: Dulbecco's modified Eagle medium; PSBMA: poly(sulfobetaine methacrylate); H_2S: hydrogen sulphide; CBS: cystathionine β-synthase; LB-I: LipoBots-inside; LB-O: LipoBots-outside; R: radius; D: diameter; MSNs: mesoporous silica nanoparticles; AuNPs: gold nanoparticles; Ni; nickel; Pt: platinum; APTES: 3-aminopropyltriethoxysilane; OTES: octyltriethoxysilane; GA: glutaraldehyde; CdS: cadmium sulfide; β-CD: β-cyclodextrin; HPAM: hyperbranched polyamide; NO: nitric oxide; ROS: reactive oxygen species; HLA_n: n represents the mass ratio of L-arginine to HPAM; DOX: doxorubicin; HF: heparin/folic acid; HFLA: heparin/folic acid/L-arginine; MTB: magneto-tactic bacteria; Fe: iron; HP: hollow microparticles; molecular motor: [5,5′-(9-(2-methyl-2,3-dihydro-1*H*-cyclopenta[*a*]naphthalen-1-ylidene)-9*H*-fluorene-3,6-diyl)diisophthalic acid]; NA: not available or not explicitly mentioned in the respective publications.

have done enough justice in evaluating MNBs for their *in vivo* use.

Numerous MNB designs have thus emerged, partly spawned by uniqueness/novelty objectives, but mostly by selective needs to control motor and cargo behavior in a biological context. Thus, presenting specific challenges such as the need to immune-mask MNBs while allowing the targeting of cancer cells in biological tissues (blood or solid tissue) having varying viscosities. Thus, the chemical tunability of MNBs, attributed to the biomaterials utilized in the fabrication of the said motors, forms the cornerstone of the immense utility of MNBs in biomedical, chemical and environmental sciences. Moreover, MNBs have shown promising utility in biomedical and allied fields resulting in the establishment of start-ups and spin-offs (Table 2) specifically focussing on the development of MNBs for varied applications. Thus, discussing the chemical editability of advanced nanomaterials transforming them from mere ''static'' entities to ''active'' and autonomous entities is essential and very topical.

Contemporary reviews by other groups cover a wide array of research foci such as biohybrid engines (Shivalkar *et al.*), Janus microrobots (Su *et al.*), deep tissue drug delivery and imaging in

Table 2 A list of start-ups and spin-offs developing MNBs for various applications

No.	Start-up/spin-off	Founding year	Platform technology	Utility	Location	Ref.
1.	Nanobots Therapeutics	2023	Enzyme driven mesoporous silica MNBs	Treatment of bladder cancer and other solid tumors	Spain	75–78
2.	AMAROB Technologies	2020	Piezoelectric material	Intra-corporeal laser surgeries	France	79 and 80
3.	Theranautilus	2020	Magnetic MNBs	Oral healthcare	India	81
4.	Nanorobotics	2019	Molecular motors	Oncology, antimicrobial, cosmetics, agriculture	Israel	82
5.	Bionaut Labs	2016	Magnetic MNBs	Therapy (neuro-oncology and neurodegeneration), microsurgery and diagnostics	USA	83
6.	Actorius Innovations and Research	2013	Magnetic antibody based multi-component system	Liquid biopsy- Circulating tumor cell capture	India	84

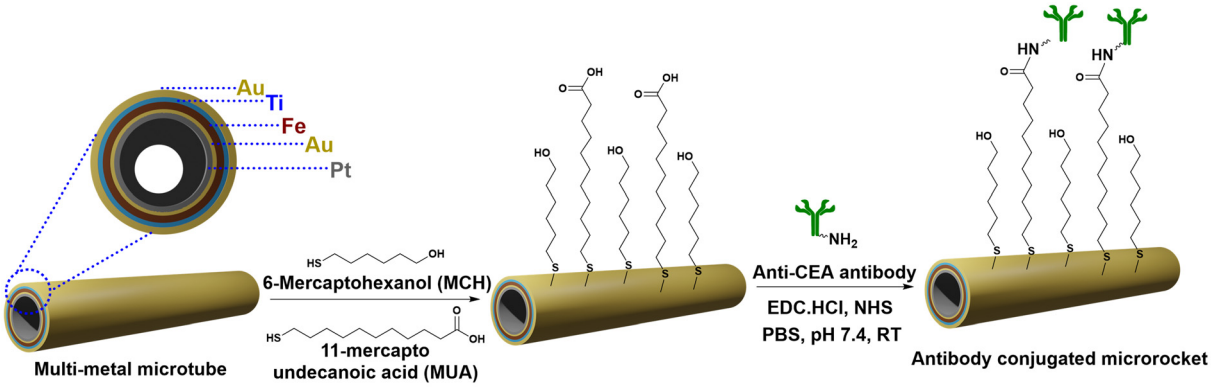

Fig. 4 Steps involved in the fabrication of a multi-metal anti-CEA antibody conjugated microrocket. Information adapted from ref. 90.

a physiological perspective (Meisami *et al.*), diagnosis and treatment (Zhang *et al.*) and magnetic MNBs (Wang *et al.*).[60–64] These reviews, while introducing the broad area of MNBs and even nanomaterials in general, overlook the potential of chemical tunability as a surface modification.

This review aims to illustrate the diversity of advanced materials used in the fabrication of MNBs. Furthermore, we highlight that the surface of the advanced materials can be chemically tuned to introduce functional moieties. Thus, through simple chemical modifications, MNBs can be fabricated to garner autonomous abilities. Next, we discuss the potential applications of MNBs as a new class of nanotherapeutics. Following this, we briefly address the biosafety and ethical concerns which may arise from using MNBs *in vivo* for therapeutic applications. Finally, we examine the limitations of the current MNBs and discuss the future directions in the field.

2. Fabrication of micro/nanobots by chemical modifications of advanced materials

A. Metals and metal oxide nanoparticles

Metal based ''passive'' or ''static'' NPs including gold, silver, platinum, quantum dots, ferric oxide (Fe_2O_3), ferrous ferric oxide (Fe_3O_4), silica and mesoporous silica NPs have been researched extensively for diagnostic, therapeutic and theranostic applications. Interestingly, metal and metal oxide NPs including gold, silver, platinum, magnesium, zinc, calcium carbonate and Fe_3O_4 can act as the carriers of therapeutic cargoes as well as the motors (catalytic portions) in the fabrication of MNBs.

Work by Khandare *et al.* on ''static'' advanced materials demonstrated diverse bio-functionality generated by altering the chemistry of iron oxide nanoparticles, carbon nanotubes and graphene nanosheets for applications in drug delivery and targeted enrichment of circulating tumor cells (CTCs).[85–89] Thus, demonstrating that libraries of advanced materials can be investigated for varied applications *via* simple surface chemical modifications. A similar extrapolation can be drawn to MNBs, wherein a library of chemical compositions with self-propulsion capabilities can be achieved *via* the chemical surface modification of ''static'' NPs transforming them into ''active micro/nano motor'' entities.

Balasubramanian *et al.* reported one of the first microrockets to have chemically conjugated antibodies on the surface.[90] They constructed multi-layered tubular microrockets *via* the step-by-step chemical vapour deposition of various metals. The foremost step included the deposition of a sacrificial photoresist layer on a silicon wafer, followed by the chemical vapour deposition of Ti, Fe, Au and Pt layers having 10 nm, 15 nm, 5 nm and 10 nm thickness respectively (Fig. 4). The nanolayers deposited on the sacrificial layer of the photoresist are under mechanical stress. Once the photoresist layer is dissolved the stress is released and the layer rolls up to form tubular microrockets. The microtubes obtained were coated with a final layer of Au to enable further surface modifications using alkanethiols including 6-mercaptohexanol (MCH) and 11-mercaptoundecanoic acid (MUA).

The free carboxyl groups of MUA were reacted with the free amine groups of the anti-carcinoembryonic antigen (anti-CEA) antibody using *N*-hydroxysuccinimide (NHS) and *N*-(3-dimethylaminopropyl)-*N*′-ethylcarbodiimide hydrochloride (EDC) to form an amide bond. Pt deposited as the innermost layer reacts with hydrogen peroxide (H_2O_2) to generate oxygen bubbles. As the bubbles detach from the surface, the microrockets are pushed forward by the resulting thrust. Bare microrockets attained a speed of 2 mm s^{-1} (a force corresponding to 250 pN) in PBS spiked with 7.5% w/v H_2O_2, while the anti-CEA antibody conjugated microrockets reached a speed of up to 150 μm s^{-1} (18 pN). Additionally, in human serum the maximum speed attained was 100 μm s^{-1} (13 pN). Thus, a microrocket capable of towing a cellular cargo in complex biological media was reported by the group for the first time.

Fe_3O_4 NPs are FDA approved advanced materials in specific applications and have been used in the fabrication of MNBs owing to their superparamagnetic susceptibility.[91] Interestingly, Fe_3O_4 NPs also demonstrate peroxidase like catalytic activity.[92,93] This dual modality has been exploited by our group previously to design carbon nanotube based microrockets for cell capture and nanobots for *in vitro* deep tissue penetration.[30,31]

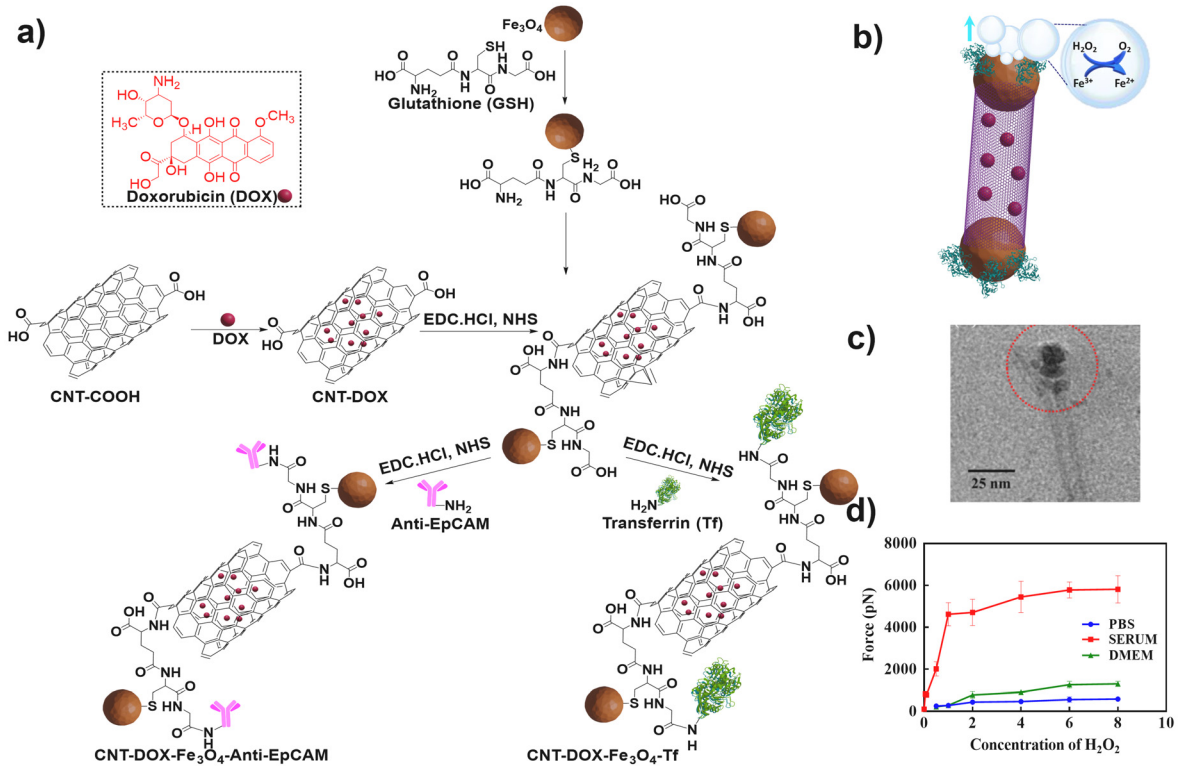

Fig. 5 (a) Steps involved in the synthesis of CNT-DOX-Fe_3O_4-Tf or CNT-DOX-Fe_3O_4-EpCAM nanobots. Information adapted from ref. 31. (b) Reaction mechanism involved in the propulsion of CNT-DOX-Fe_3O_4-Tf nanobots. Information adapted from ref. 31. (c) TEM micrograph of the CNT-DOX-Fe_3O_4-Tf nanobot. Red circle indicates the Fe_3O_4 capped end of the CNT. Reproduced from ref. 31. (d) Graphical representation of alterations in the force generated during the propulsion of nanobots in various media. Reproduced from ref. 31.

Banerjee *et al.* reported the fabrication of microrockets comprising oxidized CNTs having Fe_3O_4 NPs deposited inside the cavities and transferrin (Tf) was conjugated to the CNT surface, for the *in vitro* targeted capture of cancer cells.[30] The Fe_3O_4 NPs were entrapped inside the CNT cavities by the co-precipitation of ferrous and ferric salts in the presence of ethylene glycol and ammonia. Thereafter, Tf was conjugated using the EDC coupling reaction resulting in Tf-CNT-Fe_3O_4 microrockets. In this case, the Fe_3O_4 NPs act as nanocatalysts, wherein Fe^{3+} is converted to Fe^{2+} by H_2O_2 forming oxygen *via* a Fenton like reaction at the Fe_3O_4 and solution interface.[94] The oxygen molecules generated accumulate to form O_2 trapped bubbles. The accumulation of bubbles induces a buoyancy driven ascending motion. The speed in the upward direction was observed to be 900 μm s^{-1} and 620 μm s^{-1} in Dulbecco's modified Eagle medium (DMEM) when spiked with 8% w/w and 4% w/w H_2O_2 respectively. The drag force exerted during the ascent in 4% w/w H_2O_2 corresponds to 300 pN.

Further advancement in tapping the catalytic potential of Fe_3O_4 NPs for designing nanobots was utilized by our group to fabricate antibody conjugated nanobots targeting and penetrating tumor spheroids.[31] Oxidized CNTs were utilized as the advanced materials for loading the anticancer drug doxorubicin (DOX). The DOX loaded CNTs were covalently capped with glutathione (GSH) modified Fe_3O_4 NPs using the EDC coupling reaction. The free carboxyl groups present on the tips of CNTs react with the free amine groups of GSH present on GSH modified Fe_3O_4 NPs resulting in the formation of amide bonds.

Furthermore, the targeting ability was imparted by conjugating Tf or anti-epithelial cell adhesion molecule (anti-EpCAM) antibodies resulting in CNT-DOX-Fe_3O_4-Tf or CNT-DOX-Fe_3O_4-EpCAM nanobots (Fig. 5a–c). The nanobots propelled efficiently in phosphate buffered saline spiked with H_2O_2 as well as in DMEM and serum. H_2O_2 is present innately in the plasma in a concentration range of 0–5 μM under normal physiological conditions,[95] whereas, in cancer patients the levels are elevated up to 10 μM.[95]

Interestingly, CNT-DOX-Fe_3O_4-Tf nanobots displayed buoyancy induced propulsion as described previously (Fig. 5b). Fe_3O_4 NPs display catalytic potential in H_2O_2 solutions up to a concentration of 0.006% w/v of H_2O_2. Moreover, the propulsion speeds of the nanobots increased in serum spiked with H_2O_2 compared to PBS and DMEM. This counter-intuitive improvement in functionality was attributed to the build-up of protein coronas on the nanobots. Thus, enzymes such as catalase could potentiate the propulsion kinetics along with a decrease in the surface tension at the catalysis interface. The maximum speed obtained in serum spiked with 8% w/v H_2O_2 was 8.026 mm s^{-1} and the corresponding force was 5435 pN (Fig. 5d). Furthermore, the nanobots were designed to release DOX more efficiently in acidic environments in the presence of enzymes such as cathepsin B by the cleavage of amide bonds.

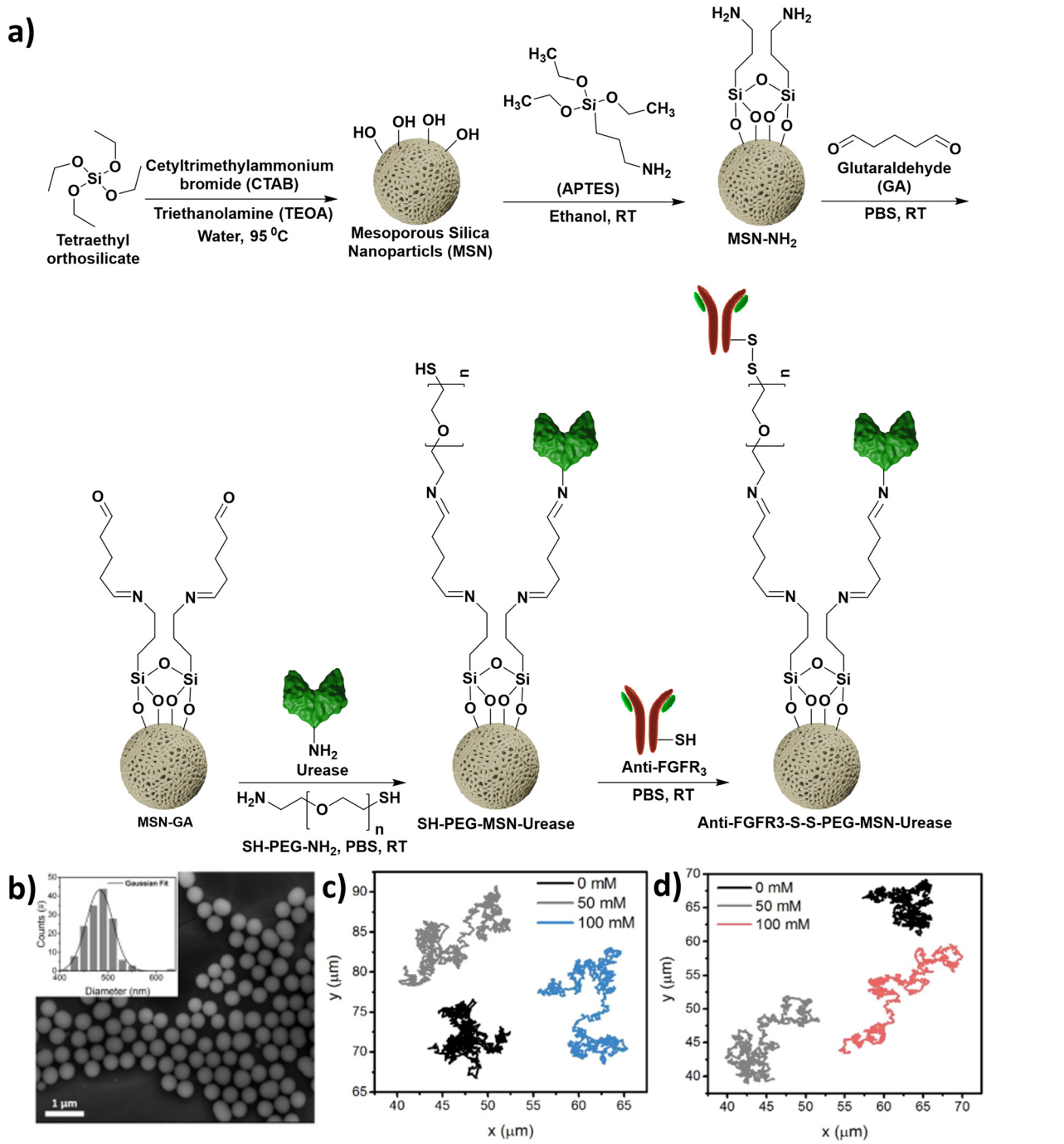

Fig. 6 (a) Steps involved in the synthesis of urease powered nanomotors. Information adapted from ref. 96. (b) SEM micrograph of MSNs. The inset represents the corresponding size distribution. Reprinted with permission from ref. 96, Copyright 2019, American Chemical Society. (c and d) Tracings of paths followed by the SH-PEG-MSN-urease nanomotors and anti-FGFR3-S-S-PEG-MSN-Urease nanomotors, respectively, in the presence of increasing concentrations of urea (0–100 mM). Reprinted with permission from ref. 96, Copyright 2019, American Chemical Society.

Mesoporous silica nanoparticles (MSNs) are biocompatible materials with the potential for further bio-chemical modifications. Particularly, in the fabrication of MNBs, MSNs can be utilized as carriers for drugs/targeting moieties or as templates to form Janus MNBs. Hortelão *et al.* reported the synthesis of nanomotors powered by urease which propel by converting urea to ammonia.[96] Mesoporous silica NPs (MSNs) comprised the carrier segments whilst urease enzyme was utilized as the motor. First, silanization of the MSNs was carried out using 3-aminoprpyltriethoxy silane (APTES), as depicted in Fig. 6a.

Subsequently, the free amines obtained post silanization were reacted with glutaraldehyde to yield imines. The glutaraldehyde modified MSNs were subsequently reacted with the free amine groups of either urease or bifunctional

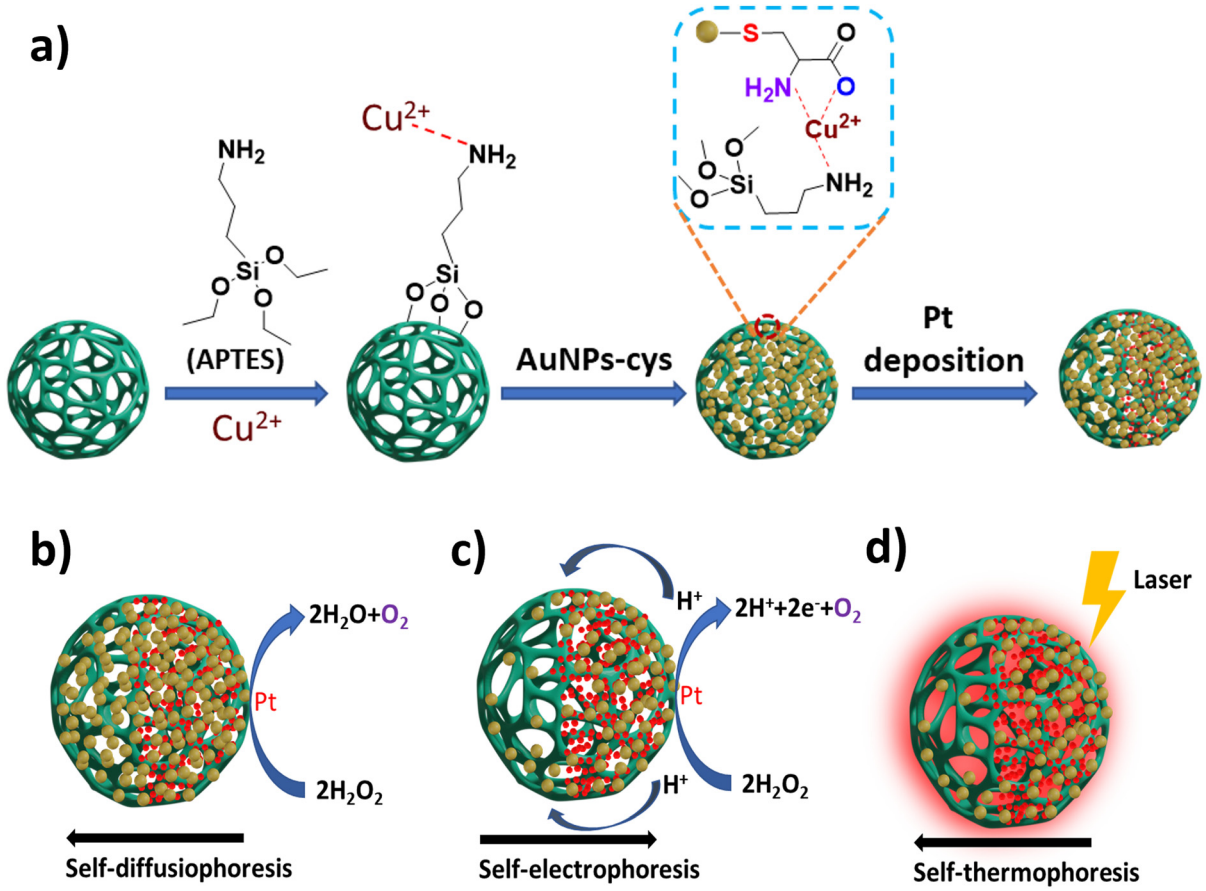

Fig. 7 (a) Schematic representation of the synthesis of core@satellite JMPA nanomotors. (b–d) Schemes representing self-diffusiophoresis, self-electrophoresis and self-thermophoresis mechanisms of JMPA nanomotors. Information adapted from ref. 66.

poly(ethylene glycol) (NH_2-PEG-SH). Finally, the thiol terminus of PEG was conjugated to the anti-fibroblast growth factor receptor 3 (anti-FGFR3) antibody (Fig. 6a). The nanomotors have uniform size distribution, and the path length travelled increases with increasing concentration of urea (Fig. 6b–d). Therefore, MSN based nanomotors can be synthesized *via* covalent surface alterations.

Xing *et al.* designed a multi-metal, multi-phoretic propulsive, pH-responsive nanomotor for biomedical applications.[66] In brief, the nanomotor was constructed by the loading of AuNPs-cys on aminated MSNs (MSNs-NH_2) through a Cu^{2+} coordination bridge. Then the monolayer of MSNs-NH_2-Cu^{2+}@AuNPs-cys was modified with PtNPs *via* physical vapor deposition to obtain the Janus (MSNs)-Pt@Au (JMPA) nanomotor (Fig. 7a). The JMPA nanomotor undergo three types of phoretic propulsion: self-diffusiophoresis, self-electrophoresis and self-thermophoresis. In the first process of self-diffusiophoresis, the JMPA nanomotor propels due to the catalytic decay of H_2O_2 by the deposited PtNPs (Fig. 7b). Elevation of the acidic pH on the surface of the MSNs in H_2O_2 causes the dissociation of AuNPs-cys-Cu^{2+} by breaking the coordination link between the amine (–NH_2) of MSNs and Cu^{2+}. Secondly, gold nanoparticles form aggregates on the surface of the MSNs due to the combination of the remaining AuNPs-cys (–NH_2) with AuNPs-cys-Cu^{2+}, leading to electron transfer from the PtNP layer to AuNPs. This generation of an electrochemical interaction between Pt and Au drives the nanomotor by self-electrophoresis (Fig. 7c). Finally, self-thermophoretic propulsion occurs due to irradiation of a laser at 670 nm on AuNP aggregates, which generate a photothermal effect and activates the nanomotor (Fig. 7d).

Peng *et al.* reported the development of Fe_2O_3 microrobots exhibiting a uniformly oriented symmetric dendrite-like arrangement synthesized through an easy and economic single-step hydrothermal reaction using only one component.[97] By gaining power from dual sources (light irradiation/magnetic field), the Fe_2O_3 microrobots undergo negative phototaxis. The photocatalysis involves a decrease in the concentration of GSH around the cancer cells owing to the H_2O_2-stimulated active generation of ROS (photo-Fenton reaction).

The two actuation modes offered by the biocompatible microrobots greatly influence the direction of their movement, thus providing synergistic assistance in prostate cancer treatment *via* photodynamic therapy.

Dekanovsky *et al.* designed an advanced class of microrobots exhibiting autonomous propulsion for eliminating pollutants, such as steroid hormones, from contaminated water sources.[98] They synthesized a self-automated microrobotic system using

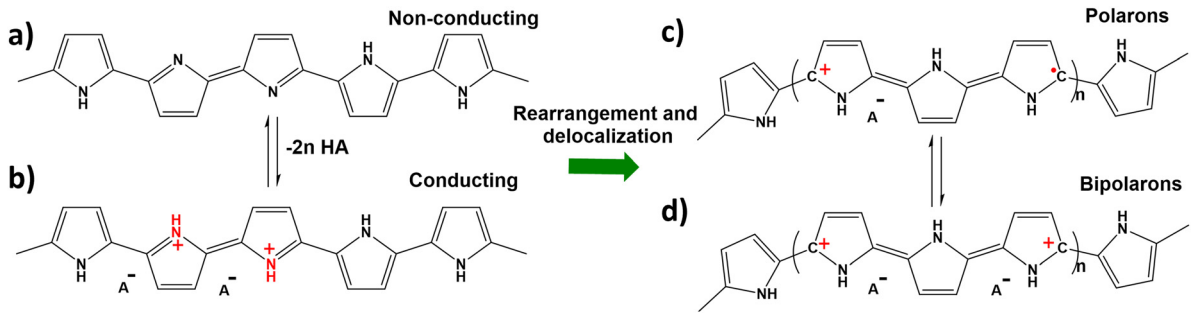

Fig. 8 (a) Pristine PPy structure in the deprotonated state, (b) protonated PPy molecule, and (c and d) polarons and bipolarons obtained after rearrangement of the protonated PPy molecule. Information adapted from ref. 98.

the electrodeposition template-assisted method. The tubular microrobot system comprised of a peripheral functional layer of conductive polymer, poly(pyrrole) (PPy), while the interior comprised of Fe_3O_4 NPs along with an innermost catalytic Pt layer. Fe_3O_4 NPs impart directional self-propulsion ability *via* an external magnetic stimulus. H_2O_2 acts as the fuel for the movement of PPy/Fe_3O_4/Pt microrobots in solution.

PPy is a conductive polymer which can undergo pH dependent structural changes (Fig. 8a–d). The protonation of PPy results in the generation of positive charge, and successive rearrangements and delocalization of charges occur. The positive PPy molecule can attract negative molecules from the solution, whereas at net zero charge aromatic molecules can be adsorbed *via* π–π interactions. This electrochemical tunability gives the MNB significant customizability of function. Owing to their versatile properties, PPy/Fe_3O_4/Pt microrobots are capable of effectively removing 70–80% of oestrogen fibres from polluted water, exploiting the phenomenon of the spider-web-like formation of oestrogen fibres at the surface. Due to a strong magnetic field response, the oestrogenic webs cling to the microrobots and can be conveniently collected from the solution. Such smartly fashioned microrobots with futuristic surface functionalities are implicated as an effective answer to the current challenges in the field of environmental remediation.

In yet another example, iron oxide metal–organic framework (MIL)-based versatile microrobots synthesized using a single-step etching process were reported.[99] The microrobots were surface-functionalized with PPy and further supplemented with methylene blue (MB) sensitizer molecules (Fig. 9a–c). The highly negative surface charge caused the microrobots to assemble at the focal point of the light source (the point of

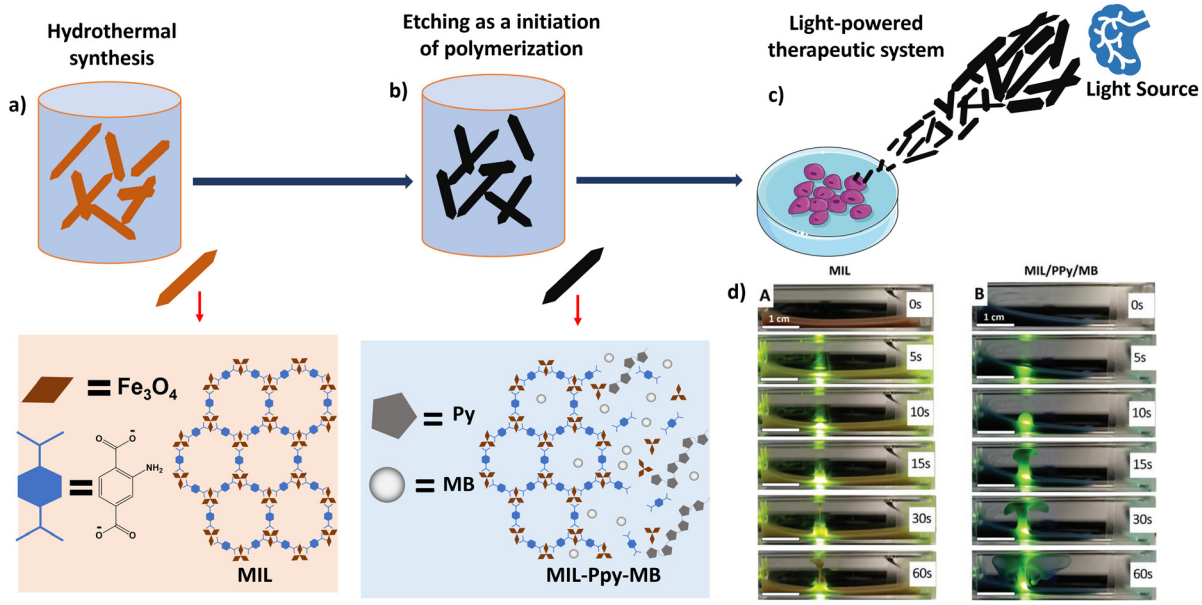

Fig. 9 Schematic representation of the synthesis of light-powered microbots. (a) Hydrothermal synthesis of the basic MIL template. Information adapted from ref. 99. (b) Polymerisation of pyrrole (Py) by etching process and incorporation of the methylene blue (MB) sensitizer. Information adapted from ref. 99. (c) Light-active accumulation of microbots and destruction of cells. Information adapted from ref. 99. Parts of the figure were drawn by using pictures from Servier Medical Art, provided by Servier, licensed under a Creative Commons Attribution 3.0 unported license. (d) Images depicting the self-assisted motion of microrobots along the beam of visible light. (A) Unmodified MIL and (B) MIL-PPy-MB microrobots. Scale bar represents 500 μm. Reproduced from ref. 99 with permission from John Wiley and Sons.

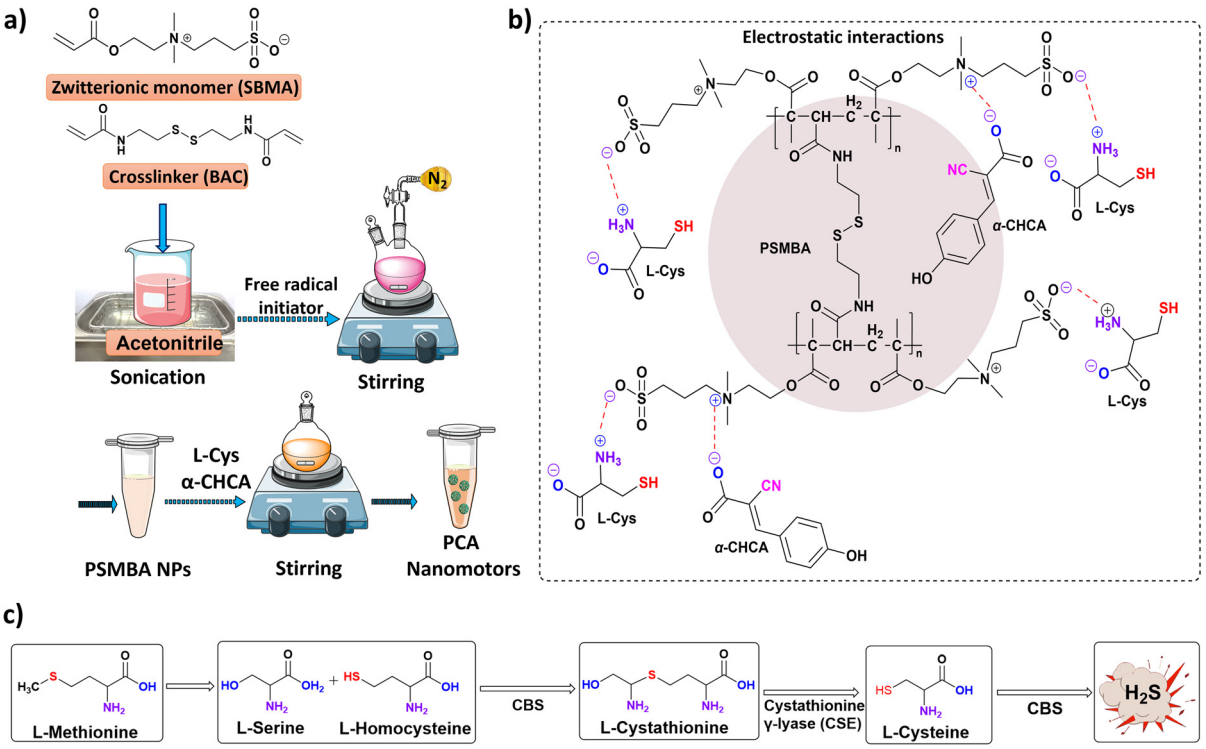

Fig. 10 (a) Schematic representation of the steps involved in the synthesis of PCA nanomotors. Information adapted from ref. 65. Parts of the figure were drawn using pictures from Servier Medical Art, provided by Servier, licensed under a Creative Commons Attribution 3.0 unported license. (b) Electrostatic interactions of L-Cys and α-CHCA with poly(sulfobetaine methacrylate) (PSMBA) NPs. (c) Steps involved in the biosynthesis of hydrogen sulfide. Information adapted from ref. 65.

maximum H^+ photogeneration), as shown in Fig. 9d. The unique blend of these light-propelled and pH-controlled microrobots is seen as offering noteworthy prospects and varied clinical applications in the field of next generation cell therapy to accomplish the therapeutic functions with a remarkable efficiency.

B. Polymer and hyper-branched polymer nanoparticles

Wan *et al.* fabricated polymeric NPs capable of inhibiting tumor growth *via* synergistic effects.[65] The zwitterionic nature of sulfobetaine methacrylate (SBMA) was used to produce an L-cysteine (L-Cys) and α-cyano-4-hydroxycinnamic acid (α-CHCA)-loaded polymer delivery system (PCA nanomotors), as shown in Fig. 10a and b. The polymeric core is formed by free radical polymerization of SBMA, resulting in the formation of disulfide bonds which are cleavable in the presence of glutathione. L-Cys and α-CHCA are loaded into the polymeric core *via* electrostatic interactions, as shown in (Fig. 10b). In the body, the biosynthetic pathway for the production of hydrogen sulfide (Fig. 10c) involves the catalysis of L-Cys by the enzyme cystathionine β-synthase (CBS).[100] In addition, CBS is up-regulated in tumor cells. The authors exploited these facts in the design of nanomotors. Thus, the PCA nanomotors displayed enhanced self-assisted motion in the presence of an increasing number of cancer cells, which was absent in the presence of non-cancerous cells.

Wan *et al.* reported a no-waste, trackable nanomotor driven by nitric oxide (NO) for therapeutic purposes (Fig. 11a–g).[70] The production of NO in the human body is caused by oxidation of the guanidine group of L-arginine by the NO synthase enzyme, the co-factor nicotinamide adenine dinucleotide phosphate (NADPH) or reactive oxygen species (ROS).[101] The five-electron oxidation of L-arginine is a two-step process; the first step involves hydroxylation of the imine group of L-arginine and the second step is the subsequent oxidation of hydroxyl L-arginine to produce citrulline and NO (Fig. 11d).

The hyper-branched polyamide/L-arginine (HLA) nanomotor was synthesized using a self-assembly approach between fluorescent hyper-branched polyamide (HPAM) and L-arginine. The binding attraction between HPAM and L-arginine is found to be electrostatic, and the negative –COOH group of L-arginine is attracted to the positive $-NH_2$ group of HPAM, leaving highly reactive (–C═NH) and ($-NH_2$) group of L-arginine outside of the nanomotor to interact with the fuel (Fig. 11a). Moreover, in an attempt to confirm the binding mechanism, the exposed the $-NH_2$ group of L-arginine of the HLA nanomotor was modified by covalent conjugation of fluorescein isothiocyanate (FITC). The fluorescence spectra of the FITC-HLA nanomotor and free FITC exhibit the same peak at 510 nm, while no peak is observed for the unconjugated HLA nanomotor. This establishes the covalent conjugation of the exposed $-NH_2$ group of the HLA nanomotor

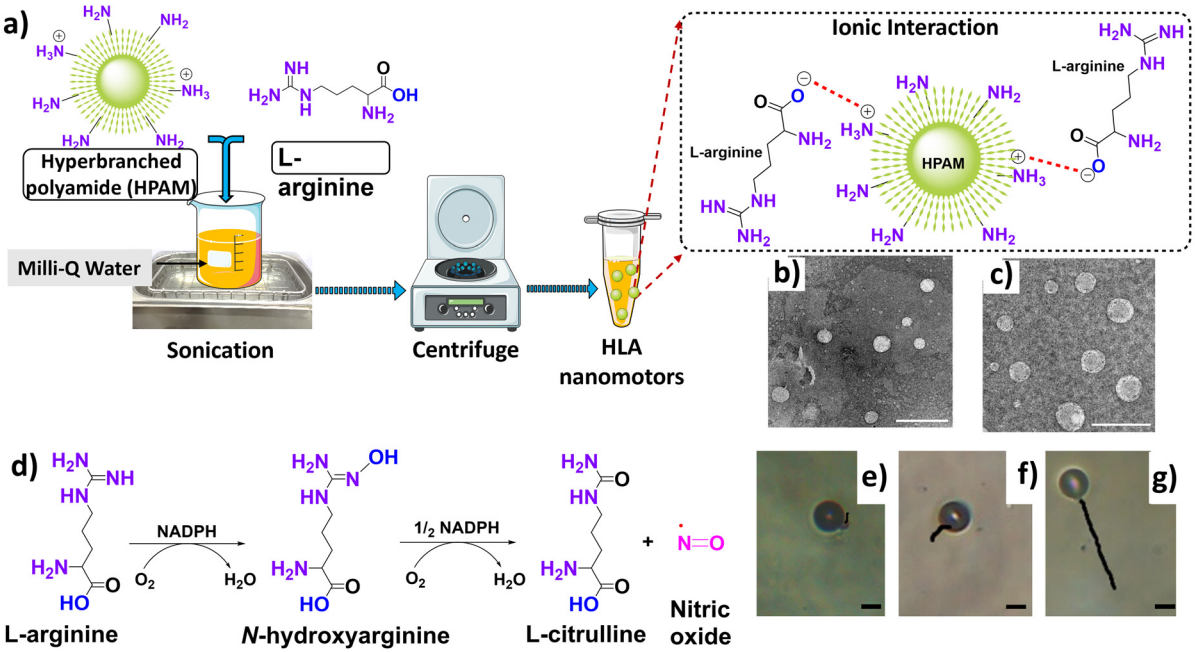

Fig. 11 (a) Steps involved in the synthesis of HLA nanomotors, with the inset representing the possible ionic interactions occurring between HPAM and L-arginine. Information adapted from ref. 70. Parts of the figure were drawn using pictures from Servier Medical Art, provided by Servier, licensed under a Creative Commons Attribution 3.0 unported license. (b and c) TEM micrographs of HLA_5 and HLA_{10} respectively (the subscripts correspond to concentration of L-arginine). Uranyl acetate was used as a negative staining agent. Scale bar represents 500 nm. Reproduced from ref. 70. (d) Steps involved in the biosynthetic pathway of nitric oxide. Information adapted from ref. 101. (e–g) Tracked path-lengths of HLA_{10} nanomotors in H_2O_2 solutions having concentration values of 5% w/v, 10% w/v and 20% w/v respectively. The trajectories were obtained over a period of 10 s. The scale bar represents 5 μm. Reproduced from ref. 70.

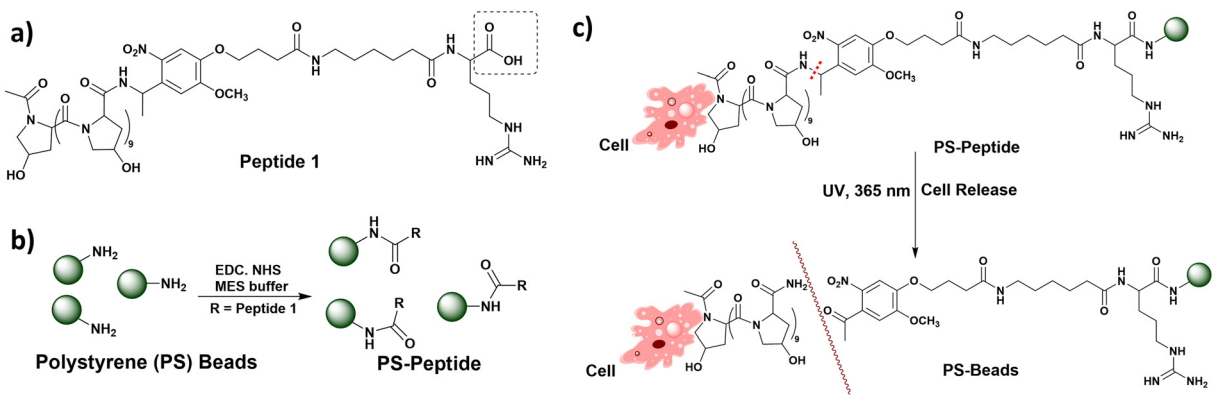

Fig. 12 (a) Peptide **1** structure. (b) Schematic representation of the reaction of aminated PS beads with the carboxylic acid group (circled in Fig. 12a) by the EDC-NHS coupling reaction. (c) Cell captured by phototaxis and release of beads from cells under UV, 365 nm. Information adapted from ref. 102.

with FITC, and reiterates the electrostatic attraction mechanism of formation of the HLA nanomotor.

The movement of nanomotors was investigated using H_2O_2 which was utilized to simulate ROS present *in vivo*. As the concentration of H_2O_2 increased, the length of the trajectories travelled by the nanomotors also increased (Fig. 11e–g). In addition, the consumption rate of arginine increases over time and the production rate of NO decreases, therefore supporting the propulsion mechanism hypothesis. The same group also reported an enhanced version of the previous nanomotors by fabricating heparin and folic acid NPs loaded with L-arginine and doxorubicin (DOX) referred to as HFLA-DOX nanomotors.[71]

C. Biohybrids comprising biological membranes or biomolecules

Weibel *et al.* reported the microscale equivalent of an ox, termed "microoxen" (Fig. 12a–c). It was fabricated using a species of unicellular algae, *Chlamydomonas reinhardtii* (CR), with two flagella known to display chemotaxis, phototaxis, geotaxis and gyrotaxis.[102] The algal cell wall is found to be rich

in peptides containing 4-hydroxyproline (4-HP). Their intrinsic surface chemistry was utilized to incorporate poly(styrene) (PS) beads modified with 4-HP peptides into the cell wall by multiple non-covalent interactions. A photocleavable group, 4-[4-(1-aminoethyl)-2-methoxy-5-nitrophenoxy]butanoic acid (NPOP), was introduced into the 4-HP peptide, and the synthesized product was denoted as peptide **1**.

Subsequently, the terminal amine groups of the PS beads were modified with peptide **1** through the EDC coupling reaction, resulting in the formation of amide bonds, and the synthesized beads were denoted as peptide **2**. In the end, the peptide **1**-modified PS bead was incubated with CR for a fixed period, and it was observed that the beads attached to the cell wall. After exposure to visible light (500 nm), CR used the flagella for motility. Negative and positive phototaxis occurred in response to a high and low intensity of light, respectively. Accordingly, a back-and-forth motion was presented by CR when placed in PDMS-based microfluidic channels, in response to light emitting diodes placed at the terminal ends of the micro-fluidic channels. Besides, the beads were released from the cell wall after exposure to UV light (365 nm). Consequently, Weibel *et al.* could successfully demonstrate the benefits of using intact biological motors for the purpose of towing, transporting and releasing loads against exposure to a physical catalyst such as light.

Another instance of biohybrid MNBs was reported by Shao *et al.*, where, counter-intuitively, the inorganic cargo component is encapsulated within a live polymorphonuclear cell and the motor is the intact cell itself.[13] In a demonstration of multi-efficient design, the mesoporous silica nanoparticles (MSNs) were first coated with *Escherichia coli* membranes (EMs) forming vesicular bodies. To integrate the 'EM-coated MSN' into the neutrophils, the coated MSNs were simply incubated with live neutrophils. The bacterial component enhanced the neutrophil uptake significantly. The EMs serve a pivotal function in the EM-MSN bodies, being attacked and engulfed by the neutrophils. The double-encapsulated MSNs now are cargo-carrying, auto-propelled biohybrid MNBs with chemotactic navigation. Shao *et al.* were able to demonstrate further that, under strong chemotaxis (effected by a large microbial load), the MNBs show ballistic motion instead of diffusive random motion. The efficient design of the MNB here is an intelligent adaptation of biohybrid design principles.

Tang *et al.* also demonstrated the success of the biohybrid MNB model in their work on exploiting intact platelets to become Janus-type MNBs by tagging the platelet surface with spacer-linked urease.[103] DOX-loading of the platelets further arms them to deliver a toxic payload to the targeted tissue/cell type. Indeed, Tang and colleagues further take advantage of a well-established interaction of platelets and a breast cancer cell line to specifically target breast cancer cells. The Janus-urease tagging of platelets, dubbed as JPL-motors (Janus platelet micromotor), was shown to have minimal to no impact on the survival and behaviour of the platelets, while allowing the chemically tuned platelets to efficiently interact with the MDA-MB-231 breast cancer cells. These JPL motors thus serve as completely biocompatible 'cell-robots'. While the urea–urease system would preferentially work efficiently in the bladder system, an appropriate targeting system would ensure the success of the MNB scheme. Like the neutrophil cell MNB model, the biocompatibility is ensured by utilization of intact, live cell systems. However, the key difference between the work presented by Shao *et al.* and Tang *et al.* is the complete encapsulation of the MNB within a live cell with chemotactic capabilities by Shao and colleagues, whereas the JPL-motor system relies on extracellular 'engines'.

Pané *et al.* disclosed the fabrication of helical-shaped robots, termed ''candybots''.[104] These millimetre-sized robots exhibited a corkscrew type of motion when exposed to an external magnetic field. The ''candybots'' were fabricated through 3D printing by utilizing the selective laser sintering (SLS) technology. The foundation was laid by the caramelized products of glucose and sucrose, while the sensitivity to the magnetic field was provided by barium ferrite ($BaF_{12}O_{19}$) microparticles. Owing to their helical shape, the ''candybots'' displayed a corkscrew like motion under the influence of an external rotating magnetic field (30 mT, 5 Hz) followed by complete disintegration upon dissolution of the caramelized sucrose. The degree of caramelization, being the rate-limiting step in the synthesis process, provided the flexibility to produce either rigid or flexible helical swimmers. It was proposed that these sucrose-based robots may serve as biocompatible and biodegradable platforms for the site-specific delivery of various particles prior to their disintegration to release the desired particles.

3. Biomedical applications

The previous sections highlighted the ability of advanced materials to be fine-tuned for surface modifications and utilize a variety of chemical and/or physical stimuli to achieve self-assisted motion. Some examples exploit the microenvironment in the target tissues. Thus, MNBs, on account of their chemical designs, can be used for multiple biomedical applications.

The anti-CEA antibody conjugated microrockets reported by Balasubramanian *et al.* have applications in the *in vitro* capture of circulating tumor cells (CTCs).[90] They demonstrated the cell capturing ability of the immune microrockets by spiking CEA positive cancer cells in human serum. The microrockets were not only able to capture and tow the cancer cells but they were successful in distinguishing CEA positive and CEA negative cells, thus demonstrating the specificity (Fig. 13a and b).

The Tf-CNT-Fe_3O_4 microrockets reported by Banerjee *et al.* (synthesis described in the previous section) were able to specifically target and enrich Tf receptor positive (TfR+) cells spiked with human peripheral blood mononuclear cells (hPBMCs) with a capture efficiency corresponding to around 85% CTCs.[30] Colon cancer cells (HCT116) labelled with green fluorescent protein (GFP) were captured by the microrockets in 5 min (Fig. 14). The force required to tow one cell was determined to be 1.88 pN using the Stokes law. As the

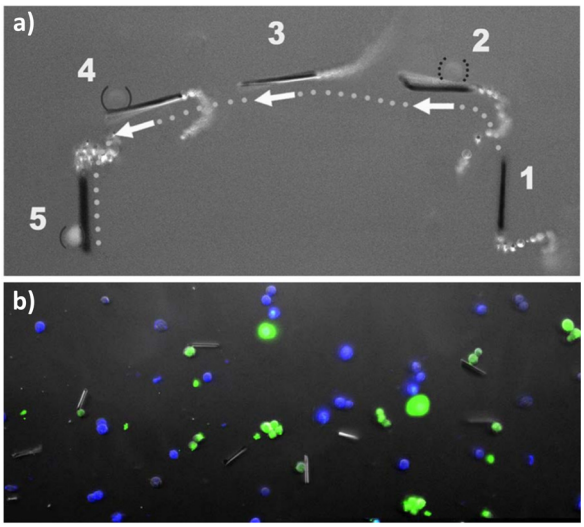

Fig. 13 (a) Images of anti-CEA antibody conjugated microrockets overlayed, showing the capture of CEA positive cells (solid parentheses). (b) Images of anti-CEA antibody conjugated microrockets after incubation with CEA positive and CEA negative cells. Reproduced from ref. 90, with permission from John Wiley and Sons.

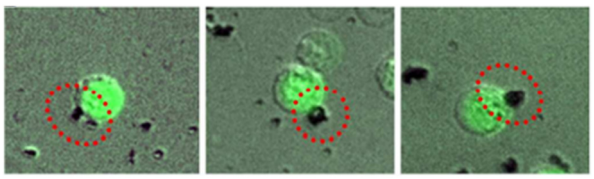

Fig. 14 Fluorescence microscope images of GFP labelled HCT116 cells captured by Tf conjugated CNT-Fe_3O_4 microrockets within 5 min. Reproduced from ref. 30.

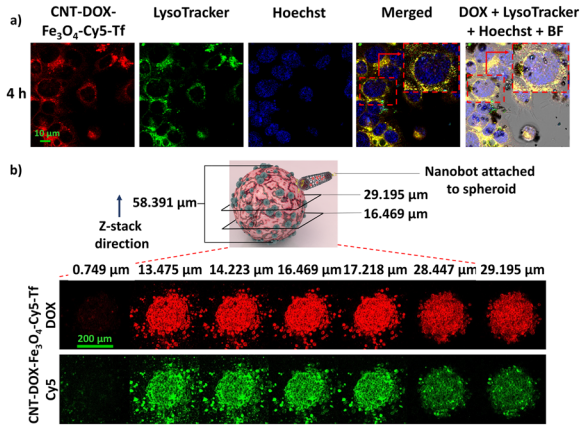

Fig. 15 (a) Fluorescence microscope images of HCT116 cells treated for 4 h with Cy5 tagged CNT-DOX-Fe_3O_4-Tf nanobots. Co-localization of LysoTracker (green) and DOX (red) signals to give a yellow color after merging. The scale bar represents 10 μm. (b) Confocal laser scanning microscopy z-stack images of HCT116 3D spheroids treated with CNT-DOX-Fe_3O_4-Cy5-Tf MNRs. The scale bar represents 200 μm. Reproduced from ref. 31.

microrockets tow the cell in the upward direction the velocity decreased to 500 μm s^{-1} in 4% H_2O_2 spiked DMEM while towing cells.

The CNT-DOX-Fe_3O_4-Tf nanobots reported by Andhari *et al.* showed application in targeted drug delivery and deep tissue penetration. The nanobots release DOX from the CNT cavities in an acidic environment (pH 5 and pH 6.5), which is further enhanced in the presence of cathepsin B. This trait of the nanobots is particularly advantageous as the TME pH is 6.5 and the lysosomal pH is around 5. Therefore, DOX is released specifically in the TME and further in the lysosomes, which was demonstrated using a fluorescent dye for tracking lysosomes and co-localization of DOX fluorescence in the lysosomes (Fig. 15a).

The CNT-DOX-Fe_3O_4-Tf and CNT-DOX-Fe_3O_4-EpCAM nanobots successfully inhibited the growth of 3D spheroids generated using HCT116 cells. Additionally, H_2O_2 levels are known to be elevated in the TME, which assists the propulsion of the nanobots and improves the tissue-penetration ability of the drug carriers. The CNT-DOX-Fe_3O_4-Tf nanobots tagged with the Cy5 fluorescent dye penetrate the HCT116 3D spheroids up to a depth of 29 μm (Fig. 15b). The deep cell/tissue penetration arising from the self-propulsion abilities, the TME specific drug release and the targeting abilities render such advanced materials as true "active seekers" of their intended site of action, thereby limiting the side-effects.

Wan *et al.* reported a zwitterionic nanobot system utilizing a dual molecule delivery strategy to induce acidotic physiology in cancer cells, thereby predisposing them to cytostasis which slows the spread and growth of cancer cells (fabrication described in previous section).[65] Enhanced tumor penetration was achieved by exploiting the greater occurrence of CBS in the TME. The release of the second molecule, α-CHCA, was designed to inhibit the removal of lactate from the cell. Cancer cells are known to drive glycolysis at a rate greater than normal healthy cells, resulting in lactic acid being accumulated (the Warburg effect).[105]

The resulting acidity, though helpful for the cancer cell to alter its microenvironment, is deleterious for the cell itself and hence requires an efflux mechanism for survival. The α-CHCA is shown to inhibit the transporter and compromise the cancer cell, resulting in the cytostatic activity of the nanobot. This innovative approach successfully exploits the TME as well as utilizes a drug combination which is non-toxic to the healthy cell, especially within the confines of healthy physiology. Furthermore, the nanobot is designed to be influenced by the relatively higher glutathione in the TME and undergo disintegration to avoid systemic accumulation.

Wan *et al.* have also addressed the two major problems in current chemotherapy methods, namely, the poor penetration of the drug, and multidrug resistance (MDR), by utilizing the physiological function of NO (Fig. 16a).[106] The production of oxidant peroxynitrite ($ONOO^-$) by reaction of NO with superoxide leads to the stimulation of active-matrix metalloproteinases (MMPs) in the solid tumor (Fig. 16b). An improvement in the penetration of drug loaded nanoparticles can be

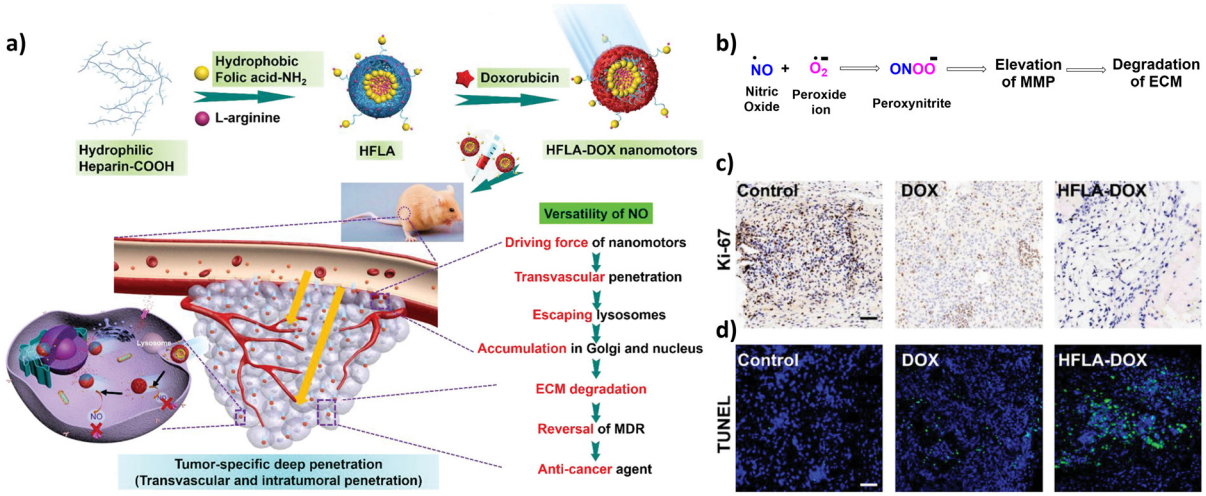

Fig. 16 (a) Schematic illustration of the fabrication of HFLA-Dox nanomotors and their mechanism of action in tumor penetration. Reproduced from ref. 106. (b) Reaction depicting the generation of peroxynitrite, resulting in degradation of the ECM. Information adapted from ref. 106. (c) Immunohistochemistry images obtained from mice bearing tumor tissues treated with free DOX and HFLA-DOX. Ki-67 was used as a proliferation marker. The brown colour indicates proliferating cells, and the blue colour indicates the nuclei. The scale bar represents 50 μm. Reproduced from ref. 106. (d) Fluorescent images obtained after performing immunofluorescence staining using terminal deoxynucleotidyl transferase dUTP nick and labelling (TUNEL). The green colour indicates apoptotic cells. The blue colour indicates the nuclei. The scale bar represents 50 μm. Reproduced from ref. 106.

possible due to the degradation of the extracellular matrix (ECM) by the MMPs. This was observed by penetration of the nanomotors in the *in vivo* models, resulting in efficient growth inhibition (Fig. 16c and d). Simultaneously, NO can inhibit P-glycoprotein (P-gp) expression and act as an efficient reverser of the MDR of the solid tumor.

Another effective approach to designing site-specific micro/nanomotors is observed in a study reported by Hortelão *et al.*, which exploits cancer site chemistry to provide for micro/nano motor propulsion as well the targeting moiety.[96] The enzyme urease takes advantage of the cancer tissue involved, in this case the urinary bladder, which would be associated with a large amount of excreted urea stored in the bladder. Urease lyses urea into carbon dioxide and ammonia, generating the thrust required for the silica NB. Conjugation of the FGF3R antibody onto a PEGylated strand on the silica NB allows the specific targeting of cancerous tissue as well as effective blocking of the FGF3 signalling pathway, resulting in loss of the proliferative and migration potential.

Gao *et al.*, provided a simplistic demonstration of the utilization of surface chemistry and site-specific propulsion, which was the first *in vivo* assessment of nanobots like these.[107] In an effort to translate the traditional chemical catalyst zinc to nanoscale activity, Gao and co-workers synthesized zinc nanorods with a protective poly(3,4-ethylenedioxythiophene) (PEDOT) coating. Under the influence of gastric fluid, in the intended target site within the stomach, zinc is catalytically active at the extremities of the nanorods. Zinc generates hydrogen from locally available hydrochloric acid. At the gastric pH value of 1.2, zinc-PEDOT nanorobots are able to penetrate the mucilaginous coat on the inner walls of the stomach and able to release their cargo of gold nanoparticles. This study illustrates the practicality of site-specific chemical tunability, which can be used for precise functions.

Dual *in vivo and ex vivo* investigations provide a platform for the detailed analysis of nanobot functioning, physio-location and kinetics, such as that reported by Wu *et al.*[108] Wu and colleagues synthesized a relatively complex micromotor system wherein physiologically active components, such as drugs and gold, were coated onto a Mg core nanoparticle. The Mg-nanoparticles by virtue of synthesis had a directional feature built-in which allowed the gaseous emission to form a 'bubble-jet'. Next the Mg-NP cluster was microencapsulated within an enteric-coated gelatin matrix to afford stability in the gastric passage.

The system was monitored using photo-acoustic computed tomography, which allowed precise tracking and kinetic study of the micromotor and payload. Once past the gastric phase, near-infrared irradiation was used to disintegrate the microcapsules and release the micromotors. The basic environment of the intestine helped sustain the activity of the Mg micromotors, which operated by decomposition of water to hydrogen gas bubbles. *In vivo* analysis demonstrated the efficacy of the micromotors in migrating through the intestines and the tumor model as well the kinetics of delivery.

Natural physiological barriers such as the epithelial or endothelial tight junctions are a restrictive step for penetration of the micro/nanobots at their target site. In this vein, Zhang *et al.* have reported a complex system involving nanogels for delivering the anticancer drug paclitaxel to cancer cells.[44] Briefly, the drug along with gelatin and iron oxide NPs are formulated into a nanogel, which was first encapsulated within *Escherichia coli* derived membrane vesicles. These vesicles were further subject to phagocytosis by competent neutrophils, allowing the vesicles to be borne by the neutrophils into the

target regions *via* extravasation. The final neutrophil-hybrid microbots ('neutrobots') are dual responsive, in that they maintain responsiveness to an external magnetic field as well the chemical gradient of signalling cytokines, sensed by the neutrophils. The use of neutrophils allows the nanomotors to access the most hard-to-reach tissue niches, where the drug can be released for maximum effect, and which in this case was an anticancer effect.

4. Biosafety and ethical concerns about micro/nanobots

As the field advances, newer materials are developed for arising therapeutic needs, and concerns regarding the ethical use of autonomous entities need to be addressed. Nauber *et al.* have discussed the factors which must be taken into consideration while the design of MNBs specifically in reproductive medicine.[109] They showcase that the materials used in the fabrication are key factors influencing biocompatibility and that the sterility of such systems must also be addressed. Insights for obtaining regulatory approvals for the *in vivo* use of MNBs have been discussed. They have highlighted that MNBs may be considered as ''combined products'' by regulatory authorities as they would fall under the category of medical devices as well as drug products if carrying a pharmaceutically active ingredient.

Along similar lines, Arvidsson *et al.* provide recommendations on the necessary regulatory changes which shall be required for the *in vivo* utility of MNBs.[110] They further highlight the environmental risks which MNBs might pose. These discussions reiterate the importance of ''quality by design'' in the fabrication of MNBs. Moreover, autonomous therapies are not limited to the microscale as surgical procedures also move towards autonomy. Yang *et al.* provide a useful guideline on the ''levels of autonomy'' in the context of the use of AIMs in medicine.[111]

Thus, considering these factors, advanced materials used in the fabrication of MNBs must be biocompatible, biodegradable and must not induce an immune response. Previously approved materials for *in vivo* use can be considered to be potential candidates for the design of MNBs. For example, PLGA NPs and phospholipid NPs can serve as the carrier segments for injectable formulations and a multitude of polymeric excipients for oral MNBs, while the catalytic segment can comprise of non-fouling chemical elements. Therefore, as rewarding as the use of MNBs may appear, the design of biocompatible and ethically sound MNBs still presents challenges that need to be overcome by the inherent traits of the advanced materials used in the synthesis of MNBs.

5. Conclusions and future perspectives

In light of the immense leap forward with regard to technological possibilities in the 'small' but important domain, the path towards ideal MNBs appears to be shorter than previously envisioned. Designing MNBs that can accomplish tasks similar to those of complex biological processes, which are often driven by multiple bio-chemical stimuli, is highly desirable and yet challenging. Despite limitations in the carrying capacity at micro/nano-scales due to the low Reynolds number fluidics, impeccable precision of targeting and activity regulation can compensate well for the shortcomings. Bio-hybrid MNBs are emerging as a superior incarnation of NP carriers, whereas synthetic MNBs are sophisticated enough to discriminate between intracellular compartments. The chemistry toolkit available today plays a powerful role in enabling multi-functional and multi-efficient MNBs.

'Artificial intelligence materials' (AIMs) in the form of MNBs, mediated by physico-chemical traits, shall offer better utilities beyond contemporary comprehensions. Such materials shall complement the possibilities that have never been imagined and anticipated, in particular where human intervention is expected to be minimal, including complex biology.

The past decade has seen advances in MNB propulsion such as the use of light, sound, fuels and catalytic enzymes selectively noted in metabolic niches such as the TME. Multi-purpose iron oxide MNBs, for instance, serve functions of propulsion, magnetic navigation, cargo-carriers, drug-conjugation substrates and even the source of free radicals useful in accelerating oxidative stress in the TME. This exemplifies that a single chemical component can be utilized to remotely program MNBs *via* physical means as well as chemical means. Chemical control of MNBs exploits biochemical pathways specific to diseased tissues, some of which have been discussed in the review. Such biosynthetic pathways and their by-products can be the starting point for the development of MNBs in the future as well.

The utility of enzymes with TME-selective fuels or the reverse, with MNB-incorporation of metabolic intermediates selective for enzymes over-expressed in the TME, is a successful strategy for exploiting the local environment. The appropriate selection of MNB base materials can also aid secondary objectives such as imparting self-limiting or self-destructive traits. Perhaps the most attractive aspect of the chemical tunability of MNBs is the synergistic effects that can be achieved with cytotoxic agents to reduce their non-specific activities.

Currently, MNBs are limited by their payload carrying capacities, immunological responses, generation of potentially toxic by-products and tissue-retention of MNB components post therapy. Progress is being made to develop approaches to overcome these drawbacks including utilization of remote physical stimuli for propulsion and the introduction of surface barriers to reduce immunological responses. While masking the metallic motor segments with biological membranes has gained popularity, it is imperative to be cautious about the unknown natural fate of these membranes and their reproducibility. In addition, the cost effectiveness and ease of manufacturing processes must also be addressed.

As we draw attention to the multimodality of a single chemical constituent of MNBs, we must also draw attention to the role of each component used to design MNBs. The

accountable utility of each chemical species shall further improve the tunability of MNBs and in-turn reassure their biosafety. Thus, the next generation MNBs must be multimodal and comprise minimal chemical species with each constituent having specific functionalities.

Moreover, we highlight that multiple start-ups and spin-offs have been recently based on the application of MNBs and thus the design of such AIMs is critical. As the field progresses, the more challenging aspects must also be discussed including the biocompatibility and fate of MNBs. In this context, the chemical constituents of the MNBs are the critical parameters that shall drive the success or failure of MNBs in the clinic. Therefore, understanding their chemical tunability is a first step in the vast array of scrutiny AIMs/MNBs must undergo before showing any breakthrough utility in medicine. As multiple groups around the world start work on the topic highlighted in the review, the efforts in this direction are accelerated.

In this context, advanced synthetic materials that would be the preferred candidates for biomedical applications are those that can be fabricated in streamlined manufacturing processes, can mimic biological membranes, and are biocompatible and biodegradable. Furthermore, irrespective of the advanced materials utilized in the fabrication of MNBs, the determination of surface properties in biologically relevant media depending on their intended application (blood, stomach, and bladder) shall assist in the corelation of expected *in vivo* effects.

To achieve the above undertakings close collaborative efforts between chemists and biologists would be required. As exemplified by the bio-orthogonal click chemistry (2022 Nobel Laureates in Chemistry, Carolyn R. Bertozzi, Morten Meldal and K. Barry Sharpless), chemical reactions can occur under physiological conditions. Similarly, the advent of the MNB era shall require an in-depth understanding of the chemical properties of advanced nanomaterials along with their biological implications.

Therefore, with regard to the *in vivo* systemic delivery of MNBs, their surface charge, interactions with proteins, chemical components of their architecture and controlled locomotion, as opposed to uncontrolled high speeds, shall play a crucial role in governing their pharmacokinetics and pharmacodynamics. Once this has been achieved, MNBs can be envisioned as true ''active seekers'' of their biological ''hits'', which may include large tissues (solid tumors), single cells (CTCs or leukemic cells), bacteria or viruses.

Author contributions

J. K. conceived the review concept. S. A., G. K., R. G. and Y. P. carried out the literature search. S. A. and G. K. drew the schematic and chemical illustrations. J. K., S. A., G. K., R. G. and Y. P. wrote and edited the manuscript. All authors have reviewed the final version of the manuscript.

Conflicts of interest

There are no conflicts of interest to declare.

Acknowledgements

The authors acknowledge the support of School of Pharmacy and School of Consciousness, Dr Vishwanath Karad MIT-World Peace University. The authors also acknowledge the resources provided by Actorius Innovations and Research India and USA, and OneCell Diagnostics India and USA.

References

1 J. Wang, *Nat. Commun.*, 2021, **12**, 7125.
2 F. Mehfuz, in *2018 International Conference on Sustainable Energy, Electronics and Computing Systems (SEEMS)*, Greater Noida, India, April 2018, pp. 1–6.
3 M. Fisher, L. Dennis and M. Webster, *Commun. ACM*, 2013, **56**, 84–93.
4 J. Torresen, *Front. Robot. AI*, 2018, **4**, 75.
5 W. Wang, L. A. Castro, M. Hoyos and T. E. Mallouk, *ACS Nano*, 2012, **6**, 6122–6132.
6 W. Gao, S. Sattayasamitsathit, J. Orozco and J. Wang, *J. Am. Chem. Soc.*, 2011, **133**, 11862–11864.
7 Y. Wang, Z. Li, A. A. Solovev, G. Huang and Y. Mei, *RSC Adv.*, 2019, **9**, 29433–29439.
8 R. Dong, Q. Zhang, W. Gao, A. Pei and B. Ren, *ACS Nano*, 2016, **10**, 839–844.
9 J. Wang, Z. Xiong, J. Zheng, X. Zhan and J. Tang, *Acc. Chem. Res.*, 2018, **51**, 1957–1965.
10 D. G. Nicholls and S. J. Ferguson, *Bioenergetics*, 2013, 197–220.
11 A. Varki, *Glycobiology*, 2017, **27**, 3–49.
12 J. L. V. Corrons, L. B. Casafont and E. F. Frasnedo, *Ann. Hematol.*, 2021, **100**, 2425–2433.
13 J. Shao, M. Xuan, H. Zhang, X. Lin, Z. Wu and Q. He, *Angew. Chem., Int. Ed.*, 2017, **56**, 12935–12939.
14 Y. Alapan, O. Yasa, O. Schauer, J. Giltinan, A. F. Tabak, V. Sourjik and M. Sitti, *Sci. Rob.*, 2018, **3**, eaar4423.
15 H. Xu, M. Medina-Sánchez, V. Magdanz, L. Schwarz, F. Hebenstreit and O. G. Schmidt, *ACS Nano*, 2018, **12**, 327–337.
16 X. Tang, Y. Yang, M. Zheng, T. Yin, G. Huang, Z. Lai, B. Zhang, Z. Chen, T. Xu, T. Ma, H. Pan and L. Cai, *Adv. Mater.*, 2023, 2211509.
17 Z. Wu, Y. Chen, D. Mukasa, O. S. Pak and W. Gao, *Chem. Soc. Rev.*, 2020, **49**, 8088–8112.
18 W. F. Paxton, K. C. Kistler, C. C. Olmeda, A. Sen, S. K. Angelo, Y. Cao, T. E. Mallouk, P. E. Lammert and V. H. Crespi, *J. Am. Chem. Soc.*, 2004, **126**, 13424–13431.
19 L. Hu, K. Tao, J. Miao and G. Grüber, *RSC Adv.*, 2016, **6**, 102513–102518.
20 Z. Ye, Y. Sun, H. Zhang, B. Song and B. Dong, *Nanoscale*, 2017, **9**, 18516–18522.
21 R. Liu and A. Sen, *J. Am. Chem. Soc.*, 2011, **133**, 20064–20067.
22 I. Santiago, L. Jiang, J. Foord and A. J. Turberfield, *Chem. Commun.*, 2018, **54**, 1901–1904.

23 S. Cao, J. Shao, H. Wu, S. Song, M. T. De Martino, I. A. B. Pijpers, H. Friedrich, L. K. E. A. Abdelmohsen, D. S. Williams and J. C. M. van Hest, *Nat. Commun.*, 2021, **12**, 2077.
24 G. Y. Karaca, F. Kuralay, E. Uygun, K. Ozaltin, S. E. Demirbuken, B. Garipcan, L. Oksuz and A. U. Oksuz, *ACS Appl. Nano Mater.*, 2021, **4**, 3377–3388.
25 J. Wu, S. Balasubramanian, D. Kagan, K. M. Manesh, S. Campuzano and J. Wang, *Nat. Commun.*, 2010, **1**, 36.
26 R. D. Wavhale, K. D. Dhobale, C. S. Rahane, G. P. Chate, B. V. Tawade, Y. N. Patil, S. S. Gawade and S. S. Banerjee, *Commun. Chem.*, 2021, **4**, 159.
27 W. Gao, R. Dong, S. Thamphiwatana, J. Li, W. Gao, L. Zhang and J. Wang, *ACS Nano*, 2015, **9**, 117–123.
28 M. Guix, A. K. Meyer, B. Koch and O. G. Schmidt, *Sci. Rep.*, 2016, **6**, 21701.
29 A. R. Morgan, A. B. Dawson, H. S. McKenzie, T. S. Skelhon, R. Beanland, H. P. W. Franks and S. A. F. Bon, *Mater. Horiz.*, 2013, **1**, 65–68.
30 S. S. Banerjee, A. Jalota-Badhwar, K. R. Zope, K. J. Todkar, R. R. Mascarenhas, G. P. Chate, G. V. Khutale, A. Bharde, M. Calderon and J. J. Khandare, *Nanoscale*, 2015, **7**, 8684–8688.
31 S. S. Andhari, R. D. Wavhale, K. D. Dhobale, B. V. Tawade, G. P. Chate, Y. N. Patil, J. J. Khandare and S. S. Banerjee, *Sci. Rep.*, 2020, **10**, 4703.
32 G. Go, J. Han, J. Zhen, S. Zheng, A. Yoo, M. J. Jeon, J. O. Park and S. Park, *Adv. Healthcare Mater.*, 2017, **6**, 1601378.
33 C. M. Oral, M. Ussia and M. Pumera, *Small*, 2022, **18**, 2202600.
34 M. Ussia, M. Urso, K. Dolezelikova, H. Michalkova, V. Adam and M. Pumera, *Adv. Funct. Mater.*, 2021, **31**, 2101178.
35 D. Pantarotto, W. R. Browne and B. L. Feringa, *Chem. Commun.*, 2008, 1533–1535.
36 X. Arqué, A. Romero-Rivera, F. Feixas, T. Patiño, S. Osuna and S. Sánchez, *Nat. Commun.*, 2019, **10**, 2826.
37 L. Wang, Y. Huang, H. Xu, S. Chen, H. Chen, Y. Lin, X. Wang, X. Liu, S. Sánchez and X. Huang, *Mater. Today Chem.*, 2022, **26**, 101059.
38 L. Wang, A. C. Hortelão, X. Huang and S. Sánchez, *Angew. Chem., Int. Ed.*, 2019, **58**, 7992–7996.
39 Y. Xing, X. Du, T. Xu and X. Zhang, *Soft Matter*, 2020, **16**, 9553–9558.
40 M. Xuan, J. Shao, X. Lin, L. Dai and Q. He, *ChemPhysChem*, 2014, **15**, 2255–2260.
41 K. Cai, S. Sun, J. Shi, C. Zhang and Y. Zhang, *Phys. Chem. Chem. Phys.*, 2021, **23**, 18893–18898.
42 Y. Tu, F. Peng, X. Sui, Y. Men, P. B. White, J. C. M. Van Hest and D. A. Wilson, *Nat. Chem.*, 2016, **9**, 480–486.
43 A. C. Hortelão, S. García-Jimeno, M. Cano-Sarabia, T. Patiño, D. Maspoch and S. Sanchez, *Adv. Funct. Mater.*, 2020, **30**, 2002767.
44 H. Zhang, Z. Li, C. Gao, X. Fan, Y. Pang, T. Li, Z. Wu, H. Xie and Q. He, *Sci. Rob.*, 2021, **6**, eaaz9519.
45 M. Hassanalian, D. Rice and A. Abdelkefi, *Prog. Aerosp. Sci.*, 2018, **97**, 61–105.
46 V. Kumar, U. H. Ko, Y. Zhou, J. Hoque, G. Arya and S. Varghese, *Adv. Intell. Syst.*, 2021, **3**, 2100005.
47 Y. Jia, P. Liao, Y. Wang and D. Sun, *Adv. Intell. Syst.*, 2022, **4**, 2270056.
48 V. S. Alabusheva, V. V. Shilovskikh, L. A. Bridenko, V. V. Gurzhiy and E. V. Skorb, *Adv. Intell. Syst.*, 2023, 2200436.
49 PDB-101: Molecule of the Month: Kinesin, **https://pdb101.rcsb.org/motm/64**, (accessed 23 March 2023).
50 S. Stolz, O. Gröning, J. Prinz, H. Brune and R. Widmer, *Proc. Natl. Acad. Sci. U. S. A.*, 2020, **117**, 14838–14842.
51 J. Wang, *Nanomachines Fundamentals and Applications*, Wiley-VCH Verlag GmbH & Co. KGaA, 1st edn, 2013, pp. 1–9.
52 H. Schlichting and K. Gersten, *Boundary-Layer Theory*, Springer-Verlag, Berlin Heidelberg, 9th edn, 2017, pp. 1–26.
53 R. F. Probstein, *Physicochemical Hydrodynamics: An Introduction*, John Wiley & Sons, Inc., 2nd edn, 1994, 109–164.
54 E. M. Purcell, *Am. J. Phys.*, 1977, **45**, 3–11.
55 J. Yu, B. Wang, X. Du, Q. Wang and L. Zhang, *Nat. Commun.*, 2018, **9**, 3260.
56 R. Toy, P. M. Peiris, K. B. Ghaghada and E. Karathanasis, *Nanomedicine*, 2014, **9**, 121–134.
57 J. M. Morachis, E. A. Mahmoud and A. Almutairi, *Pharmacol. Rev.*, 2012, **64**, 505–519.
58 S. Hauert, S. Berman, R. Nagpal and S. N. Bhatia, *Nano Today*, 2013, **8**, 566.
59 J. Khandare, M. Calderón, N. M. Dagia and R. Haag, *Chem. Soc. Rev.*, 2012, **41**, 2824–2848.
60 S. Shivalkar, P. Chowdhary, T. Afshan, S. Chaudhary, A. Roy, S. K. Samanta and A. K. Sahoo, *Colloids Surf., B*, 2023, **222**, 113054.
61 H. Su, S. Li, G. Z. Yang and K. Qian, *Adv. Healthcare Mater.*, 2022, 2202391.
62 A. H. Meisami, M. Abbasi, S. Mosleh-Shirazi, A. Azari, A. M. Amani, A. Vaez and A. Golchin, *Eur. J. Pharmacol.*, 2022, **926**, 175011.
63 Y. Zhang, Y. Zhang, Y. Han and X. Gong, *Micromachines*, 2022, **13**, 648.
64 L. Wang, Z. Meng, Y. Chen and Y. Zheng, *Adv. Intell. Syst.*, 2021, **3**, 2000267.
65 M. Wan, Z. Liu, T. Li, H. Chen, Q. Wang, T. Chen, Y. Tao and C. Mao, *Angew. Chem., Int. Ed.*, 2021, **60**, 16139–16148.
66 Y. Xing, M. Zhou, T. Xu, S. Tang, Y. Fu, X. Du, L. Su, Y. Wen, X. Zhang and T. Ma, *Angew. Chem., Int. Ed.*, 2020, **59**, 14368–14372.
67 L. Yang, Y. Zhao, X. Xu, K. Xu, M. Zhang, K. Huang, H. Kang, H. Chu Lin, Y. Yang and D. Han, *Angew. Chem., Int. Ed.*, 2020, **59**, 17697–17704.
68 L. Wang, M. Marciello, M. Estévez-Gay, P. E. D. Soto Rodriguez, Y. Luengo Morato, J. Iglesias-Fernández, X. Huang, S. Osuna, M. Filice and S. Sánchez, *Angew. Chem., Int. Ed.*, 2020, **59**, 21080–21087.

69 J. Muñoz, M. Urso and M. Pumera, *Angew. Chem., Int. Ed.*, 2022, **61**, e202116090.
70 M. Wan, H. Chen, Q. Wang, Q. Niu, P. Xu, Y. Yu, T. Zhu, C. Mao and J. Shen, *Nat. Commun.*, 2019, **10**, 966.
71 M. M. Wan, H. Chen, Z. Da Wang, Z. Y. Liu, Y. Q. Yu, L. Li, Z. Y. Miao, X. W. Wang, Q. Wang, C. Mao, J. Shen and J. Wei, *Adv. Sci.*, 2021, **8**, 2002525.
72 T. Gwisai, N. Mirkhani, M. G. Christiansen, T. T. Nguyen, V. Ling and S. Schuerle, *Sci. Rob.*, 2022, **7**, eabo0665.
73 X. Ma, X. Wang, K. Hahn and S. Sánchez, *ACS Nano*, 2016, **10**, 3597–3605.
74 L. Ribovski, Q. Zhou, J. Chen, B. L. Feringa, P. Van Rijn and I. S. Zuhorn, *Chem. Commun.*, 2020, **56**, 8774–8777.
75 Nanobots Therapeutics, **https://www.nanobotstx.com/**, (accessed 22 March 2023).
76 A. C. Hortelao, C. Simó, M. Guix, S. Guallar-Garrido, E. Julián, D. Vilela, L. Rejc, P. Ramos-Cabrer, U. Cossío, V. Gómez-Vallejo and T. Patiño, *Sci. Rob.*, 2021, **6**, eabd2823.
77 A. Llopis-Lorente, A. Garciá-Fernández, N. Murillo-Cremaes, A. C. Hortelaõ, T. Patinõ, R. Villalonga, F. Sancenón, R. Martínez-Máñez and S. Sánchez, *ACS Nano*, 2019, **13**, 12171–12183.
78 A. C. Hortelao, R. Carrascosa, N. Murillo-Cremaes, T. Patino and S. Sánchez, *ACS Nano*, 2019, **13**, 429–439.
79 AMAROB Technologies – Making Surgery Better!, **https://amarob.com/**, (accessed 22 March 2023).
80 S. Lescano, M. Rakotondrabe and N. Andreff, in *IEEE/RSJ International Conference on Intelligent Robots and Systems (IROS)*, Hamburg, Germany, December 2015, 1994–1999.
81 Theranautilus, **https://www.theranautilus.com/**, (accessed 22 March 2023).
82 Nanorobotics, **https://nanorobotics.tech/**, (accessed 21 March 2023).
83 Bionaut—Precision micro-technology, the future of healthcare., **https://bionautlabs.com/**, (accessed 21 March 2023).
84 OncoDiscover® | Circulating Tumor Cell Test, **https://www.oncodiscover.com/**, (accessed 21 March 2023).
85 S. S. Banerjee, K. J. Todkar, G. V. Khutale, G. P. Chate, A. V. Biradar, M. B. Gawande, R. Zboril and J. J. Khandare, *J. Mater. Chem. B*, 2015, **3**, 3931–3939.
86 S. Nandi, N. R. Kale, V. Takale, G. C. Chate, M. Bhave, S. S. Banerjee and J. J. Khandare, *J. Mater. Chem. B*, 2020, **8**, 1852–1862.
87 N. Kale, S. Nandi, A. Patil, Y. Patil, S. Banerjee and J. Khandare, *Biomater. Sci.*, 2020, **8**, 5729–5738.
88 A. Patil, S. Nandi, N. Kale, C. Bobade, S. Banerjee, Y. Patil and J. Khandare, *Nanoscale*, 2021, **13**, 17473–17485.
89 B. Singh, S. Arora, A. D'Souza, N. Kale, G. Aland, A. Bharde, M. Quadir, M. Calderón, P. Chaturvedi and J. Khandare, *J. Mater. Chem. B*, 2021, **9**, 2946–2978.
90 S. Balasubramanian, D. Kagan, C. M. Jack Hu, S. Campuzano, M. J. Lobo-Castañon, N. Lim, D. Y. Kang, M. Zimmerman, L. Zhang and J. Wang, *Angew. Chem., Int. Ed.*, 2011, **50**, 4161–4164.
91 J. S. Weinstein, C. G. Varallyay, E. Dosa, S. Gahramanov, B. Hamilton, W. D. Rooney, L. L. Muldoon and E. A. Neuwelt, *J. Cereb. Blood Flow Metab.*, 2010, **30**, 15–35.
92 L. Gao, J. Zhuang, L. Nie, J. Zhang, Y. Zhang, N. Gu, T. Wang, J. Feng, D. Yang, S. Perrett and X. Yan, *Nat. Nanotechnol.*, 2007, **2**, 577–583.
93 Y. Gao, G. Wang, H. Huang, J. Hu, S. M. Shah and X. Su, *Talanta*, 2011, **85**, 1075–1080.
94 S. S. Lin and M. D. Gurol, *Environ. Sci. Technol.*, 1998, **32**, 1417–1423.
95 H. J. Forman, A. Bernardo and K. J. A. Davies, *Arch. Biochem. Biophys.*, 2016, **603**, 48–53.
96 A. C. Hortelao, R. Carrascosa, N. Murillo-Cremaes, T. Patino and S. Sánchez, *ACS Nano*, 2019, **13**, 429–439.
97 X. Peng, M. Urso, J. Balvan, M. Masarik and M. Pumera, *Angew. Chem., Int. Ed.*, 2022, **61**, e202213505.
98 L. Dekanovsky, B. Khezri, Z. Rottnerova, F. Novotny, J. Plutnar and M. Pumera, *Nat. Mach. Intell.*, 2020, **2**, 711–718.
99 L. Dekanovsky, Y. Ying, J. Zelenka, J. Plutnar, S. M. Beladi-Mousavi, I. Křížová, F. Novotný, T. Ruml and M. Pumera, *Adv. Funct. Mater.*, 2022, **32**, 2205062.
100 P. Rose, P. K. Moore and Y. Z. Zhu, *Cell. Mol. Life Sci.*, 2017, **74**, 1391.
101 E. B. Manukhina, H. F. Downey and R. T. Mallet, *Exp. Biol. Med.*, 2006, **231**, 343–365.
102 D. B. Weibel, P. Garstecki, D. Ryan, W. R. DiLuzio, M. Mayer, J. E. Seto and G. M. Whitesides, *Proc. Natl. Acad. Sci. U. S. A.*, 2005, **102**, 11963–11967.
103 S. Tang, F. Zhang, H. Gong, F. Wei, J. Zhuang, E. Karshalev, B. E. F. De vila, C. Huang, Z. Zhou, Z. Li, L. Yin, H. Dong, R. H. Fang, X. Zhang, L. Zhang and J. Wang, *Sci. Rob.*, 2020, **5**, eaba6137.
104 S. Gervasoni, A. Terzopoulou, C. Franco, A. Veciana, N. Pedrini, J. T. Burri, C. de Marco, E. C. Siringil, X. Z. Chen, B. J. Nelson, J. Puigmartí-Luis and S. Pané, *Adv. Mater.*, 2020, **32**, 2005652.
105 R. J. DeBerardinis and N. S. Chandel, *Nat. Metab.*, 2020, **2**, 127–129.
106 M. M. Wan, H. Chen, Z. Da Wang, Z. Y. Liu, Y. Q. Yu, L. Li, Z. Y. Miao, X. W. Wang, Q. Wang, C. Mao, J. Shen and J. Wei, *Adv. Sci.*, 2021, **8**, 2002525.
107 W. Gao, R. Dong, S. Thamphiwatana, J. Li, W. Gao, L. Zhang and J. Wang, *ACS Nano*, 2015, **9**, 117–123.
108 Z. Wu, L. Li, Y. Yang, P. Hu, Y. Li, S. Y. Yang, L. V. Wang and W. Gao, *Sci. Rob.*, 2019, **4**, eaax0613.
109 R. Nauber, S. R. Goudu, M. Goeckenjan, M. Bornhäuser, C. Ribeiro and M. Medina-Sánchez, *Nat. Commun.*, 2023, **14**, 728.
110 R. Arvidsson and S. F. Hansen, *Environ. Sci.: Nano*, 2020, **7**, 2875–2886.
111 G. Z. Yang, J. Cambias, K. Cleary, E. Daimler, J. Drake, P. E. Dupont, N. Hata, P. Kazanzides, S. Martel, R. V. Patel, V. J. Santos and R. H. Taylor, *Sci. Rob.*, 2017, **2**, eaam8638.

